

## Supramolecular Catalysis of Unimolecular Rearrangements: Substrate Scope and Mechanistic Insights

Dorothea Fiedler, Herman van Halbeek, Robert G. Bergman, and  
Kenneth N. Raymond\*

Contribution from the Department of Chemistry, University of California,  
Berkeley, California 94720-1460

Received April 12, 2006; E-mail: raymond@socrates.berkeley.edu

**Abstract:** A cavity-containing metal–ligand assembly is employed as a catalytic host for the 3-aza Cope rearrangement of allyl enammonium cations. Upon binding, the rates of rearrangement are accelerated for all substrates studied, up to 850-fold. Activation parameters were measured for three enammonium cations in order to understand the origins of acceleration. Those parameters reveal that the supramolecular structure is able to reduce both the entropic and enthalpic barriers for rearrangement and is highly sensitive to small structural changes of the substrate. The space-restrictive cavity preferentially binds closely packed, preorganized substrate conformations, which resemble the conformations of the transition states. This hypothesis is also supported by quantitative NOE studies of two encapsulated substrates, which place the two reacting carbon atoms in close proximity. The capsule can act as a true catalyst, since release and hydrolysis facilitate catalytic turnover. The question of product hydrolysis was addressed through detailed kinetic studies. We conclude that the iminium product must dissociate from the cavity interior and the assembly exterior before hydroxide-mediated hydrolysis, and propose the intermediacy of a tight ion pair of the polyanionic host with the exiting product.

### Introduction

Inspired by nature's ability to control and manipulate chemical reactions by means of steric confinement and precisely positioned functional group interactions, synthetic chemists have developed cavity-containing structures, which could potentially fulfill similar functions. Lehn, Cram, and Pedersen introduced crown ethers and cryptands as very simple enzyme mimics.<sup>1,2</sup> Starting in the 1970s, significant advances were made by using the naturally occurring cyclodextrins as molecular hosts for chemical reactivity.<sup>3–9</sup> However, as the scale and complexity of the target reactions and their products increase, the preparation of catalytic cavitands in a covalent fashion becomes very difficult, involving costly multistep syntheses that often produce only milligram yields of material.<sup>10–12</sup> For these reasons, the use of self-assembly is gaining popularity: large and complex structures can be obtained through the self-assembly of relatively simple subunits. These subunits are programmed to form one

exclusive supramolecular structure, and the utilization of weak and reversible interactions between the components, such as hydrogen bonds or metal–ligand interactions, allows for the self-correction and formation of the most favorable thermodynamic product.<sup>13,14</sup> By binding a reactive organometallic transition metal catalyst into such molecular containers, an active site can be installed.<sup>15–20</sup> Alternatively, the supramolecular host can act as the catalyst itself. Bimolecular catalysis can occur when two reactive partners are bound within the same capsule and their relative encounter frequencies are thus increased.<sup>21–25</sup> Phase-transfer catalysis can be achieved when the solubility properties of the capsule exterior differ notably from those of the interior environment.<sup>26</sup>

- (1) Cram, D. J. *Angew. Chem., Int. Ed. Engl.* **1988**, *27*, 1009–1020.
- (2) Lehn, J.-M. *Angew. Chem., Int. Ed. Engl.* **1988**, *27*, 89–112.
- (3) Takahashi, K. *Chem. Rev.* **1998**, *98*, 2013–2034.
- (4) Breslow, R.; Guo, T. *J. Am. Chem. Soc.* **1988**, *110*, 5613–5617.
- (5) Breslow, R.; Anslyn, E. *J. Am. Chem. Soc.* **1989**, *111*, 8931–8932.
- (6) Breslow, R.; Schmuck, C. *J. Am. Chem. Soc.* **1996**, *118*, 6601–6606.
- (7) Breslow, R.; Zhang, X.; Xu, R.; Maletic, M. *J. Am. Chem. Soc.* **1996**, *118*, 11678–11679.
- (8) Breslow, R.; Huang, Y.; Zhang, X.; Yang, J. *Proc. Natl. Acad. Sci. U.S.A.* **1997**, *94*, 11156–11158.
- (9) Breslow, R.; Dong, S. D. *Chem. Rev.* **1998**, *98*, 1997–2012.
- (10) Coolen, H. K. A. C.; van Leeuwen, P. W. N. M.; Nolte, R. J. M. *J. Am. Chem. Soc.* **1995**, *117*, 11906–11913.
- (11) Clyde-Watson, Z.; Vidal-Ferran, A.; Twyman, L. J.; Nakash, M.; Sanders, J. K. M. *New J. Chem.* **1998**, 493–502.
- (12) Mattei, F.; Diederich, F. *Helv. Chim. Acta* **1997**, *80*, 1555–1588.

- (13) Yeh, R. M.; Davis, A. V.; Raymond, K. N. In *Comprehensive Coordination Chemistry II*; Meyer, T. J., Ed.; Elsevier Ltd.: Oxford, U.K., 2004; pp 327–355.
- (14) Hof, F.; Craig, S. L.; Nuckolls, C.; Rebek, J., Jr. *Angew. Chem., Int. Ed.* **2002**, *41*, 1488–1508.
- (15) Merlau, M. L.; Mejia, M. P.; Nguyen, S. T.; Hupp, J. T. *Angew. Chem., Int. Ed.* **2001**, *40*, 4239–4242.
- (16) Slagt, V. F.; Reek, J. N. H.; Kamer, P. C. J.; van Leeuwen, P. W. N. M. *Angew. Chem., Int. Ed.* **2001**, *40*, 4271–4274.
- (17) Slagt, V. F.; van Leeuwen, P. W. N. M.; Reek, J. N. H. *Angew. Chem., Int. Ed.* **2003**, *42*, 5619–5623.
- (18) Slagt, V. F.; Kamer, P. C. J.; van Leeuwen, P. W. N. M.; Reek, J. N. H. *J. Am. Chem. Soc.* **2004**, *126*, 1526–1536.
- (19) Slone, R. V.; Hupp, J. T. *Inorg. Chem.* **1997**, *36*, 5422–5423.
- (20) Wilkinson, M. J.; van Leeuwen, P. W. N. M.; Reek, J. N. H. *Org. Biomol. Chem.* **2005**, *3*, 2371–2383.
- (21) Kang, J. M.; Rebek, J., Jr. *Nature* **1997**, *385*, 50–52.
- (22) Kang, J. M.; Santamaria, J.; Hilmersson, G.; Rebek, J., Jr. *J. Am. Chem. Soc.* **1998**, *120*, 3650–3656.
- (23) Chen, J.; Rebek, J., Jr. *Org. Lett.* **2002**, *4*, 327–329.
- (24) Yoshizawa, M.; Takeyama, Y.; Kusukawa, T.; Fujita, M. *Angew. Chem., Int. Ed.* **2002**, *41*, 1347–1349.
- (25) Yoshizawa, M.; Takeyama, Y.; Okano, T.; Fujita, M. *J. Am. Chem. Soc.* **2003**, *125*, 3243–3247.

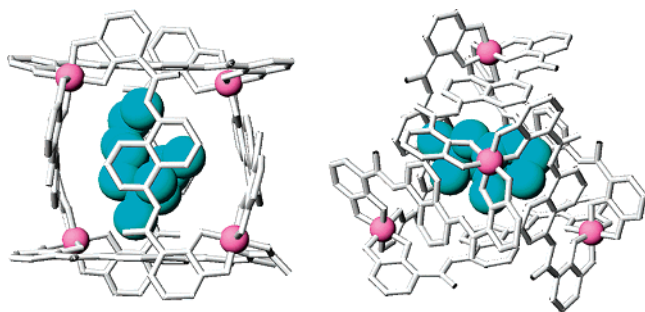


**Figure 1.** CAChe model of the  $M_4L_6$  supramolecular assembly, encapsulating an enammonium substrate. Left: View down the two-fold axis. Right: View down the three-fold axis. The guest molecule is shown in space-filling view.

The most common limitation in applying these host templates as catalytic containers is product inhibition. Since the design of the cavity relies on the shape complementarity with the reaction transition state and/or reaction products, the latter tend to associate with the host interior with similar or higher binding strength, thereby preventing catalytic turnover. Despite these difficulties, the number of catalytic scaffolds for bimolecular reactions or phase-transfer reactions is increasing, but catalytic cavities for *unimolecular* reactions are still very rare. We have previously described the use of a metal–ligand assembly as a catalytic host for unimolecular rearrangements.<sup>27</sup> Here we expand on our previous report, accounting for the origins of the observed rate accelerations and providing mechanistic insight into the separate steps involved in the catalytic cycle.

## Results and Discussion

**Identification of a Suitable Reaction: 3-Aza Cope Rearrangement.** Raymond and co-workers have developed supramolecular metal–ligand assemblies of  $M_4L_6$  stoichiometry ( $M = Ga^{3+}, Al^{3+}, Fe^{3+}, Ge^{4+}, Ti^{4+}, L = 1,5$ -bis(2',3'-dihydroxybenzamido)naphthalene).<sup>28–31</sup> In these structures, the four metal atoms are located on the vertices of the tetrahedron, while six bis-bidentate catecholamide ligands span the edges (Figure 1). Though composed of achiral components, the overall structure of the tetrahedron is chiral. The chirality is a result of the tris-bidentate coordination at each metal center, leading to either  $\Delta$  or  $\Lambda$  configuration, and due to strong mechanical coupling between the metal centers through the rigid ligands, the tetrahedra are homochiral (with either  $\Delta, \Delta, \Delta, \Delta$ - or  $\Lambda, \Lambda, \Lambda, \Lambda$ -configuration) and resolvable.<sup>32,33</sup> The metal–ligand assemblies have provided rich host–guest chemistry: a large variety of monocationic guest molecules can be encapsulated into the hydrophobic cavity, ranging from simple alkylammonium ions<sup>28</sup> to cationic organometallic species.<sup>34,35</sup>

In pursuing supramolecular catalysis, a chemical transformation of a cationic substrate which is compatible with the

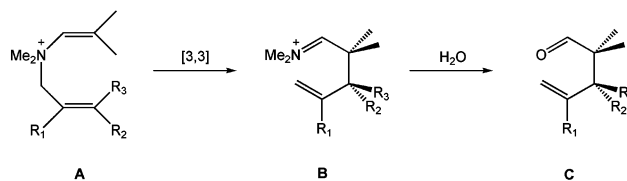


**Figure 2.** General reaction scheme of the 3-aza Cope rearrangement. Starting from the enammonium cation **A**, [3,3] sigmatropic rearrangement leads to iminium cation **B**, which then hydrolyzes to the aldehyde, **C**.

supramolecular host needed to be identified. The cationic 3-aza Cope rearrangement seemed to be most suitable to be carried out in the finite environment of the  $M_4L_6$  assembly.<sup>36–38</sup> The 3-aza Cope (or aza Claisen) reaction is a member of the [3,3] class of sigmatropic rearrangements and occurs thermally in *N*-allyl enamine systems with varying degrees of facility, depending on structural features.<sup>36,37,39,40</sup> Whereas neutral allylic enamines rearrange to  $\delta$ -ene imines at rather elevated temperatures (170–250 °C), the corresponding protonated, Lewis acid coordinated, or quaternized molecules tend to rearrange at considerably milder temperatures (20–120 °C),<sup>41</sup> making these reactions suitable for complex molecule syntheses. A catalytic enantioselective variant, however, still remains to be developed.<sup>42,43</sup>

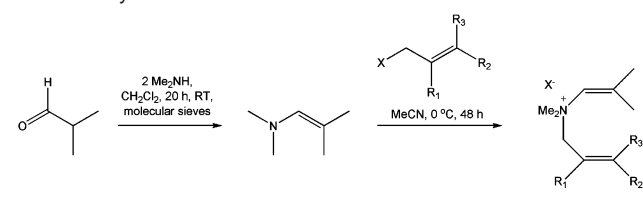
The substrates for the cationic 3-aza Cope rearrangement are enammonium cations (**A**). These cations should bind to the cavity interior because they closely resemble analogous ammonium cations, such as  $NMe_2Pr_2^+$ , which are known to strongly associate with the assembly cavity. Sigmatropic rearrangement leads to iminium cations (**B**), which are subsequently hydrolyzed to the corresponding  $\gamma, \delta$ -unsaturated aldehydes (**C**) (Figure 2). Since neutral molecules are only very weakly, if at all, bound by the supramolecular host, we thereby hope to circumvent the problem of product inhibition. The hydrolysis step could potentially be followed by binding of more substrate, enabling catalytic turnover.

A range of enammonium substrates varying in size, shape, and substitution pattern was investigated (Table 1). All enammonium salts were synthesized by alkylation of *N,N*-dimethylisobutenylamine with the corresponding allyl bromides or allyl tosylates, and were obtained as hygroscopic solids in very good yields.

**Encapsulation and Rate Acceleration.** All of the substrates, even the sterically more demanding **8** and **9**, were encapsulated by the metal–ligand assembly. This is most easily observed by <sup>1</sup>H NMR spectroscopy: shielding by the naphthalene moiety of the ligand scaffold causes an upfield shift of the guest resonances by 2–3 ppm, and placement into the chiral cavity causes enantiotopic groups to become diastereotopic. Enammonium cation **1** ( $R_1, R_2, R_3 = H$ ), for example, quantitatively yielded the host–guest complex [**1**· $Ga_4L_6$ ]<sup>11–</sup>, as confirmed

(26) Ito, H.; Kusukawa, T.; Fujita, M. *Chem. Lett.* **2000**, 598–599.  
 (27) Fiedler, D.; Bergman, R. G.; Raymond, K. N. *Angew. Chem., Int. Ed.* **2004**, *43*, 6748–6751.  
 (28) Caulder, D. L.; Powers, R. E.; Parac, T. N.; Raymond, K. N. *Angew. Chem., Int. Ed.* **1998**, *37*, 1840–1843.  
 (29) Caulder, D. L.; Raymond, K. N. *J. Chem. Soc., Dalton Trans.* **1999**, 1185–1200.  
 (30) Caulder, D. L.; Brückner, C.; Powers, R. E.; König, S.; Parac, T. N.; Leary, J. A.; Raymond, K. N. *J. Am. Chem. Soc.* **2001**, *123*, 8923–8938.  
 (31) Davis, A. V.; Raymond, K. N. *J. Am. Chem. Soc.* **2005**, *127*, 7912–7919.  
 (32) Ziegler, M.; Davis, A. V.; Johnson, D. W.; Raymond, K. N. *Angew. Chem., Int. Ed.* **2003**, *42*, 665–668.  
 (33) Terpin, A.; Ziegler, M.; Johnson, D. W.; Raymond, K. N. *Angew. Chem., Int. Ed.* **2001**, *40*, 157–160.

(34) Fiedler, D.; Leung, D.; Bergman, R. G.; Raymond, K. N. *J. Am. Chem. Soc.* **2004**, *126*, 3674–3675.  
 (35) Leung, D.; Fiedler, D.; Bergman, R. G.; Raymond, K. N. *Angew. Chem., Int. Ed.* **2004**, *43*, 963–966.  
 (36) Walters, M. A. *J. Org. Chem.* **1996**, *61*, 978–983.  
 (37) Przheval'skii, N. M.; Grandberg, I. I. *Russ. Chem. Rev.* **1987**, *56*, 477–491.  
 (38) Elkik, E.; Francesch, C. *Bull. Soc. Chim.* **1968**, *3*, 903–910.  
 (39) Opitz, G. *Justus Liebigs Ann. Chem.* **1961**, 122–132.  
 (40) Blechert, S. *Synthesis* **1989**, 71–82.  
 (41) Nubbemeyer, U. *Top. Curr. Chem.* **2005**, *244*, 149–213.  
 (42) Enders, D.; Knopp, M.; Schiffrers, R. *Tetrahedron: Asymmetry* **1996**, *7*, 1847–1882.  
 (43) Nubbemeyer, U. *Synthesis* **2003**, *7*, 961–1008.

**Table 1.** Synthesis of the Various Enammonium Salts


R <sub>1</sub>	R <sub>2</sub>	R <sub>3</sub>	X <sup>-</sup>	compound
H	H	H	Br	<b>1-Br</b>
Me	H	H	Br	<b>2-Br</b>
H	Et	H	Br	<b>3-Br</b>
H	H	Et	OTs	<b>4-OTs</b>
H	<i>n</i> -Pr	H	OTs	<b>5-OTs</b>
H	H	<i>n</i> -Pr	OTs	<b>6-OTs</b>
H	<i>i</i> -Pr	H	OTs	<b>7-OTs</b>
H	<i>n</i> -Bu	H	OTs	<b>8-OTs</b>
H	TMS	H	OTs	<b>9-OTs</b>
H	Me	Me	Br	<b>10-Br</b>

by NMR spectroscopy (Figure 3); the enantiotopic methyl groups on the nitrogen become diastereotopic upon binding, and a total of four upfield-shifted methyl resonances at 0.24,  $-0.03$ ,  $-0.60$ , and  $-1.08$  ppm are displayed for the host-guest complex. Additional confirmation of the 1:1 stoichiometry is obtained by ESI-mass spectrometry, in which peaks corresponding to a 1:1 host-guest complex are observed.

The rates of rearrangement were measured for the free and encapsulated enammonium cations to explore potential changes in substrate reactivity which may occur upon encapsulation. All rearrangements displayed clean first-order kinetics at 50 °C in buffered solution (pD = 8.00). In all cases, though, the encapsulated substrates rearranged much faster (Table 2). The highest rate acceleration was observed for the isopropyl-substituted enammonium cation **7**; binding into the host interior resulted in a rate increase by almost 3 orders of magnitude.

Interestingly, the trend of higher rate accelerations with an increase in steric demand of the guest molecule is not monotonic. There appears to be an “optimal fit” for substrate **7**, whereas accelerations for the larger substrates **8** and **9** drop off significantly. In addition, there are notable differences in the acceleration of the trans- and cis-substituted stereoisomers

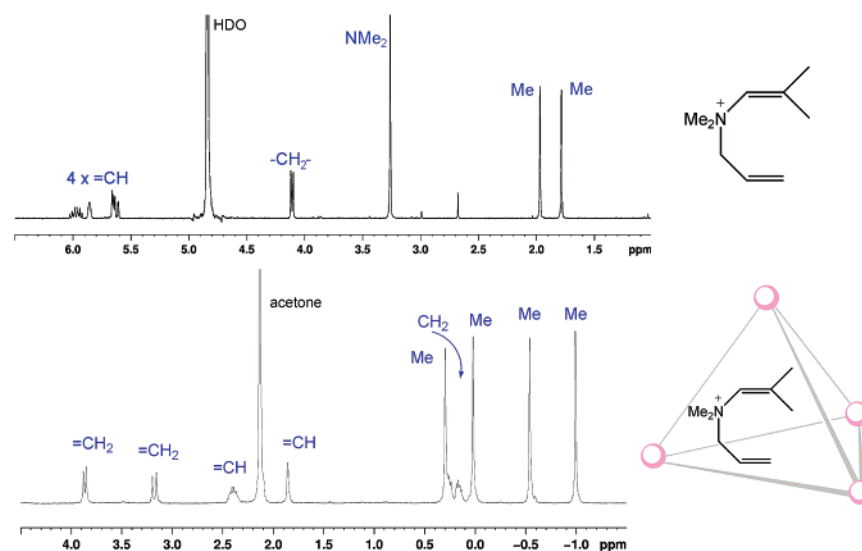
**Table 2.** Rate Constants for Free ( $k_{\text{free}}$ ) and Encapsulated ( $k_{\text{encaps}}$ ) Rearrangements (Measured at 50 °C in D<sub>2</sub>O) and Their Acceleration Factors

compound	R <sub>1</sub>	R <sub>2</sub>	R <sub>3</sub>	$k_{\text{free}}$ ( $\times 10^{-5} \text{ s}^{-1}$ )	$k_{\text{encaps}}$ ( $\times 10^{-5} \text{ s}^{-1}$ )	acceleration
<b>1-Br</b>	H	H	H	3.49	16.3	5
<b>2-Br</b>	Me	H	H	7.61	198	26
<b>3-Br</b>	H	Et	H	3.17	446	141
<b>4-OTs</b>	H	H	Et	1.50	135	90
<b>5-OTs</b>	H	<i>n</i> -Pr	H	4.04	604	150
<b>6-OTs</b>	H	H	<i>n</i> -Pr	1.69	74.2	44
<b>7-OTs</b>	H	<i>i</i> -Pr	H	0.37	316	854
<b>8-OTs</b>	H	<i>n</i> -Bu	H	3.97	222	56
<b>9-OTs</b>	H	TMS	H	0.033	1.17	35
<b>10-Br</b>	H	Me	Me	6.3	331	53

(**3** vs **4**, and **5** vs **6**). Not only the size but also the shape of the guests seem to be important in achieving optimal rate accelerations. This phenomenon of shape selectivity is not unprecedented for the M<sub>4</sub>L<sub>6</sub> assembly, and aspects of this type of selectivity have been discussed before.<sup>34,35</sup>

The observed rate enhancements might potentially be due to the cavity's more hydrophobic environment. Control experiments, however, in which the free rearrangement of **1** was monitored showed no significant solvent dependence on the rate ( $k_{\text{D}_2\text{O}} = 3.49 \times 10^{-5} \text{ s}^{-1}$ ,  $k_{\text{MeOD}} = 3.62 \times 10^{-5} \text{ s}^{-1}$ ,  $k_{\text{CDCl}_3} = 3.84 \times 10^{-5} \text{ s}^{-1}$ ). In fact, the larger substrates **8** and **9** rearranged more slowly in methanol than in aqueous solution. The prospect that the host assembly's negative charge was causing the rate acceleration was ruled out by adding salt (2 M KCl) in the absence of the assembly, which again did not result in a notable increase in rate for the free rearrangement ( $k_{\text{KCl}} = 4.02 \times 10^{-5} \text{ s}^{-1}$ ).

**Origins of Acceleration: Determination of Activation Parameters.** To investigate the origin of the observed rate accelerations, the activation parameters were measured for substrates **3**, **4**, and **7** for the free and the encapsulated rearrangements. The obtained parameters for the free rearrangement of substrate **3**, for example, are  $\Delta H^\ddagger = 23.1(\pm 0.8) \text{ kcal/mol}$  and  $\Delta S^\ddagger = -8(\pm 2) \text{ eu}$ . These values are similar to those reported in the literature for related systems,<sup>44</sup> and the highly organized transition state required for the rearrangement is mirrored in the negative entropy of activation. To ensure that

**Figure 3.** <sup>1</sup>H NMR spectra of **1-Br** (top) and [1CGa<sub>4</sub>L<sub>6</sub>]<sup>11-</sup> (bottom), illustrating the effects of encapsulation.

**Table 3.** Summary of Activation Parameters for **3**, **4**, and **7**, Free and Encapsulated

substrate	compound	solvent	$\Delta H^{\ddagger}$ [kcal mol <sup>-1</sup> ]	$\Delta S^{\ddagger}$ [cal mol <sup>-1</sup> K <sup>-1</sup> ]
	<b>3</b>	D <sub>2</sub> O	23.1 (8)	-8 (2)
	<b>3</b>	C <sub>6</sub> D <sub>5</sub> Cl	23.4 (5)	-5 (2)
	<b>4</b>	D <sub>2</sub> O	23.0 (4)	-10 (1)
	<b>7</b>	D <sub>2</sub> O	23.6 (3)	-11 (1)
	encaps. [3C Ga <sub>4</sub> L <sub>6</sub> ] <sup>11-</sup>	D <sub>2</sub> O	23.0 (9)	+2 (3)
	encaps. [4C Ga <sub>4</sub> L <sub>6</sub> ] <sup>11-</sup>	D <sub>2</sub> O	21.8 (7)	-5 (2)
	encaps. [7C Ga <sub>4</sub> L <sub>6</sub> ] <sup>11-</sup>	D <sub>2</sub> O	22.6 (9)	-1 (2)

this negative entropy of activation was not an artifact of solvation changes specific to the aqueous medium, the activation parameters for **3** were also measured in C<sub>6</sub>D<sub>5</sub>Cl, again revealing a negative entropy of activation (Table 3). The encapsulated reaction of [3C Ga<sub>4</sub>L<sub>6</sub>]<sup>11-</sup> in water gave a very similar value for the enthalpy of activation,  $\Delta H^{\ddagger} = 23.0(\pm 0.9)$  kcal/mol. The entropy of activation, in contrast, differed remarkably by almost 10 eu, with  $\Delta S^{\ddagger} = +2(\pm 3)$  eu. The activation parameters are summarized in Table 3.

Consideration of the activation parameters for the different encapsulated substrates reveals that the reasons for supramolecular catalysis are more complex than simply a reduction of the entropy of activation, since different effects are observed for substrates **3**, **4**, and **7**. While the rate acceleration for the encapsulated **3** was exclusively due to lowering the entropic barrier, a smaller  $\Delta S^{\ddagger}$  is also observed for **4** and **7**, but for the latter two the enthalpic barrier to rearrangement is also decreased. It is possible that, for those two substrates, binding into the narrow confines of the metal–ligand assembly induces some strain on the bound molecules, thereby raising their ground-state energies compared to those of the unbound substrates. Even though the differences in the activation parameters are small, they are certainly real. It is especially interesting to note that the two stereoisomers **3** and **4** respond differently to the effects of encapsulation.

An illustration of the high sensitivity of the supramolecular host to guest stereochemistry (and vice versa) are the differences in chemical shift for the bound guest substrates **3** and **4** (Figure 4). The terminal methyl groups (Me<sup>trans</sup>) are separated by more than 0.7 ppm for [3C Ga<sub>4</sub>L<sub>6</sub>]<sup>11-</sup> versus [4C Ga<sub>4</sub>L<sub>6</sub>]<sup>11-</sup> and resonate at 0.21 and -0.52 ppm, respectively. For the unbound **3** and **4**, the chemical shifts of these methyl groups are essentially identical. This seems to imply that their averaged positions within the host cavity differ significantly from each other. A similar effect is experienced by the methylene protons on the ethyl substituent (CH<sub>2</sub><sup>E</sup>); again, a large separation in their chemical shifts can be observed (Figure 4).

Taken together, these results imply that the host assembly can selectively bind preorganized, reactive conformations of the substrates, and these “exclusive conformations” are dependent on the size and shape of the entering guest substrate. The space-restrictive host cavity allows for encapsulation of only tightly packed conformers, closely resembling the conformations of the transition states. The predisposed conformers, which have already lost several rotational degrees of freedom, are selected from an equilibrium mixture of all possible conformers, and thus the entropic barrier for rearrangement decreases. Added strain that is induced by squeezing the ground state into the tight cavity is reflected by a lowered enthalpic barrier. This effect of preorganization and induced strain becomes more significant for the larger substrates, which fit more tightly in the host cavity. If the optimal fit of the reactant transition state with the host cavity is exceeded, however, rate accelerations drop off again, as illustrated by substrates **8** and **9**.

#### Evidence for Encapsulated Ground-State Preorganization.

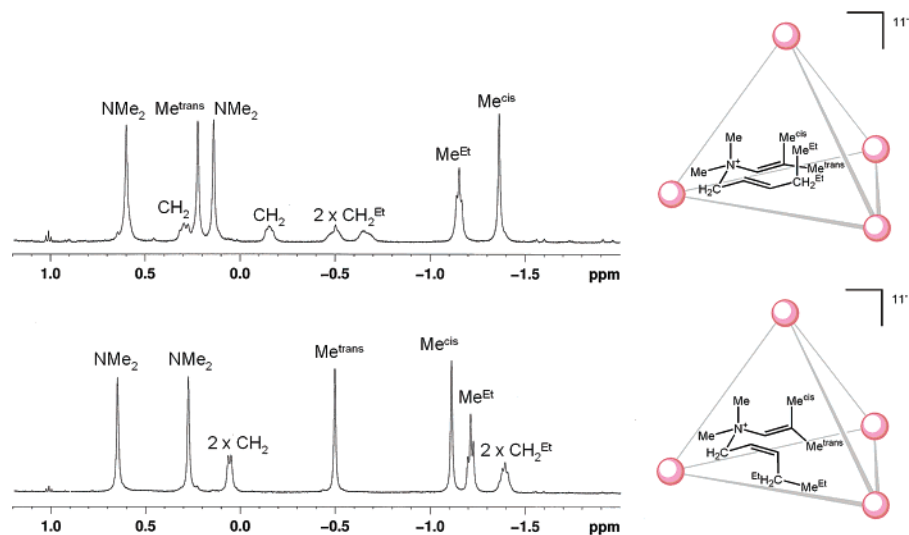
The 2D NOESY spectra of [3C Ga<sub>4</sub>L<sub>6</sub>]<sup>11-</sup> and [4C Ga<sub>4</sub>L<sub>6</sub>]<sup>11-</sup> corroborate the effect of preorganization into reactive conformations in the host–guest systems (Figure 5 and Supporting Information). The encapsulated enammonium cation **4**, for example, displays strong NOE correlations between protons at the two ends of the molecule, while unbound **4** shows no such dipolar couplings between the distal alkyl chains. These correlations would be anticipated for a tight, closely packed conformation of the bound substrate.<sup>45</sup>

To obtain more quantitative information about the exact orientation of the bound guest molecules, NOE growth rates for selected resonances in [3C Ga<sub>4</sub>L<sub>6</sub>]<sup>11-</sup> and [4C Ga<sub>4</sub>L<sub>6</sub>]<sup>11-</sup> were determined. Assuming that the initial rate approximation is valid (a linear NOE growth), the magnitude of an enhancement between two spins A and B after a period  $\tau$  will be proportional to the cross-relaxation rate, which in turn depends on the distance  $r_{AB}^{-6}$ . Using a known internal distance  $r_{XY}$  as a reference, and determining the NOE growth rates  $\sigma$  for that reference and the unknown distance, the unknown distance  $r_{AB}$  can be calculated according to  $r_{AB} = r_{XY}(\sigma_{XY}/\sigma_{AB})^{1/6}$ .<sup>46</sup> Even though the method bears several uncertainties, the success of the approach relies on the insensitivity of the calculated  $r_{AB}$  to the experimental accuracy, due to the  $r^{1/6}$  dependence (a factor of 2 error in the growth rate corresponds to only ~10% error in the distance measurement).

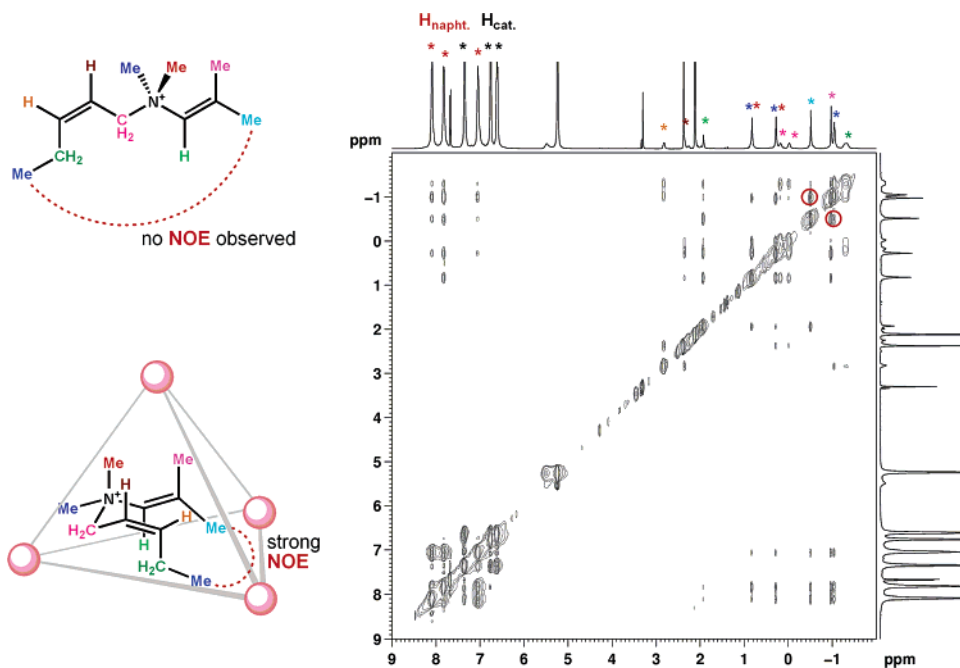
(44) Jolidon, S.; Hansen, H.-J. *Helv. Chim. Acta* **1977**, *60*, 978–1032.

(45) The short mixing time of 90 ms ensures that no correlations due to spin diffusion are observed.

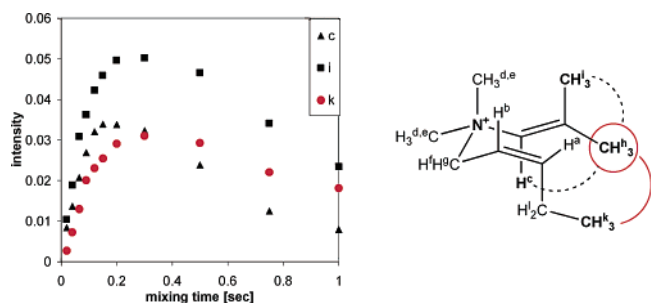
(46) Neuhaus, D.; Williamson, M. P. *The Nuclear Overhauser Effect in Structural and Conformational Analysis*, 2nd ed.; VCH Publishers: New York, 2001.



**Figure 4.** Comparison of the  $^1\text{H}$  NMR spectra of  $[\text{3CGa}_4\text{L}_6]^{11-}$  and  $[\text{4CGa}_4\text{L}_6]^{11-}$ . Significant differences in chemical shifts for the encapsulated guest can be noted, implying a different orientation for the distinct substrates.



**Figure 5.** 2D NOESY spectrum of  $[\text{4CGa}_4\text{L}_6]^{11-}$  in a  $\text{D}_2\text{O}/\text{MeOD}$  mixture (70:30) recorded at  $-10\text{ }^\circ\text{C}$ , mixing time 90 ms. Indicated in red are selected NOE correlations. The correlation between the methyl groups at the two distal ends of the molecule is a remarkable demonstration of the cavity's enforcement of a compressed and folded guest conformation.



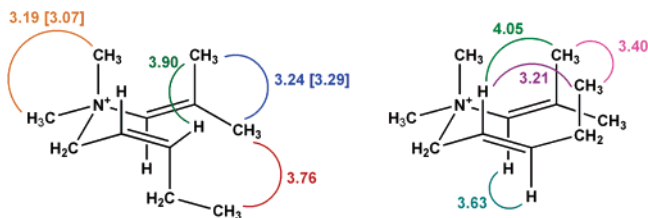
**Figure 6.** NOE buildup curves for  $[\text{4CGa}_4\text{L}_6]^{11-}$ . Remarkable is the correlation between  $\text{CH}_3^{\text{h}}$  and  $\text{CH}_3^{\text{k}}$ ; the two distal methyl groups must be held at close proximity.

Figure 6 depicts a plot of NOE cross-peak intensity vs mixing time  $\tau$  for a selected diagonal peak of  $[\text{4CGa}_4\text{L}_6]^{11-}$  and shows the typical NOE cross-peak growth for large, slowly tumbling

molecules. One remarkable correlation is the NOE between  $\text{CH}_3^{\text{h}}$  and  $\text{CH}_3^{\text{k}}$  (highlighted in red). This NOE is not observed for the unbound substrate and again illustrates the close packing of the bound guest molecule.

Quantification of the NOE growth rate yields a distance of  $3.76\text{ \AA}$  between the two methyl groups,  $\text{CH}_3^{\text{h}}$  and  $\text{CH}_3^{\text{k}}$ . Similarly, the distance between  $\text{H}^{\text{a}}$  and  $\text{CH}_3^{\text{i}}$  was determined to be  $3.90\text{ \AA}$  (Figures 6 and 7). In an analogous fashion, the NOE growth rates for  $[\text{4CGa}_4\text{L}_6]^{11-}$  were translated into distances as indicated in Figure 7.

For both averaged conformations (of **3** and **4**), the measured distances illustrate the close proximity between the two distal ends of the guest molecules, bringing the two bond-forming C atoms into contact distances. In fact, employing MM3 modeling and restricting several intramolecular distances to the calculated



**Figure 7.** Derived intramolecular distances for  $[4\text{C Ga}_4\text{L}_6]^{11-}$  (left) and  $[3\text{C Ga}_4\text{L}_6]^{11-}$  (right). Calculated distances are denoted in parentheses. Distances between methyl groups refer to a pseudoatom located in the center of the plane of the three hydrogen atoms.

values furnishes conformations of **3** and **4** in which the two reacting C atoms are less than 4 Å apart. The NOE measurements thus demonstrate that the metal–ligand assembly indeed enforces the binding of preorganized, reactive conformations.

**Catalytic Turnover.** Since one of our main goals was the design of catalytic scaffolds, the question arose as to whether the  $\text{M}_4\text{L}_6$  supramolecular assembly would also be able to mediate the aza Cope rearrangement catalytically. The stoichiometric experiments had shown that, in all cases of the host-mediated 3-aza Cope rearrangement, the iminium cations (**B**) hydrolyzed to the corresponding aldehydes (**C**), leaving behind an “empty” cavity.<sup>47</sup> The empty cavity should be able to bind more substrate and should therefore make it possible to carry out the reaction under catalytic conditions. When the reaction was conducted in the presence of 13 mol % catalyst relative to enammonium substrate, truly catalytic behavior of the supramolecular host was revealed. Increasing the catalyst loading from 13 to 27 to 40 mol % resulted in the expected rate accelerations; the observed initial rate constants at 25 °C are  $k_{13 \text{ mol } \%} = 0.64 \times 10^{-4} \text{ s}^{-1}$ ,  $k_{27 \text{ mol } \%} = 1.17 \times 10^{-4} \text{ s}^{-1}$ , and  $k_{40 \text{ mol } \%} = 1.80 \times 10^{-4} \text{ s}^{-1}$  (Figure 8).

An inhibition experiment with  $\text{NEt}_4^+$  further supports the idea of the supramolecular assembly providing a catalytic cavity for rearrangement.  $\text{NEt}_4^+$  has a very high affinity for the assembly interior and will essentially displace any other guest molecule. Addition of 8 equiv of  $\text{NEt}_4^+$  led to almost complete inhibition of the catalytic activity of the supramolecular host (Figure 8). Based on these results, the catalytic cycle illustrated in Figure 9 is proposed: (1) The restricted space of the host assembly allows for the binding of only closely packed conformers of enammonium substrates. (2) The rearrangement proceeds with significant acceleration within the boundaries of the metal–ligand assembly, due to lowered enthalpic and entropic barriers. (3) Equilibration of the rearranged product with the bulk solution is followed by hydrolysis to the corresponding aldehyde. This enables catalytic turnover by regeneration of the empty assembly which can bind additional substrate.

**Iminium Hydrolysis: Inside or Outside the Capsule?** One question that the proposed catalytic cycle did not address is that of iminium hydrolysis. Does water enter the host cavity and hydrolyze the iminium products to the corresponding aldehydes in the interior, or is dissociation of the iminium products necessary before hydrolysis can take place? With the goal of optimizing the supramolecular catalyst and eventually designing

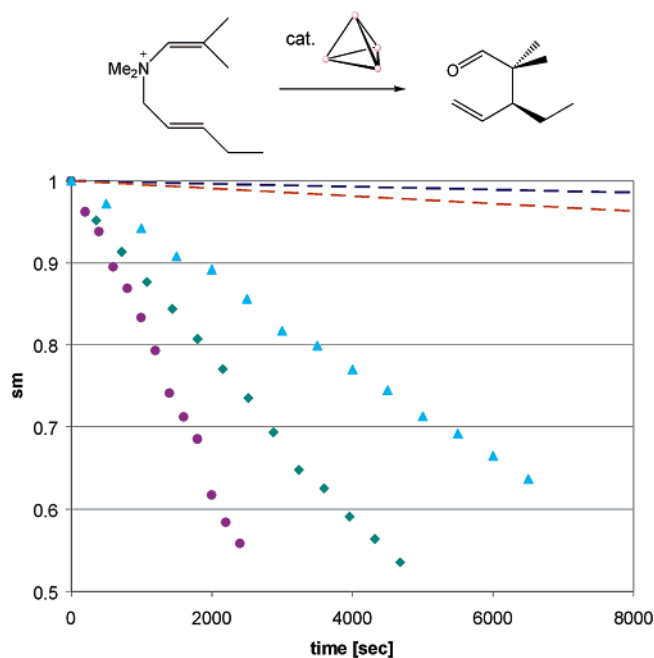


**Figure 8.** Initial rates for the catalytic 3-aza Cope rearrangement of  $[3\text{C Ga}_4\text{L}_6]^{11-}$ . Purple ●, 40% catalyst loading; green ◆, 27% catalyst loading; light blue ▲, 13% catalyst loading; orange --, 40% catalyst loading, inhibited with 8 equiv of  $\text{NEt}_4^+$ ; dark blue --, uncatalyzed reaction. “sm” denotes starting material, as determined by integration of the  $^1\text{H}$  NMR signals.

other catalytic assemblies for different chemical transformations, this issue needed to be examined.

The system of choice for these studies was host–guest complex  $[10\text{C Ga}_4\text{L}_6]^{11-}$ . Unlike most other bound enammonium substrates, the rearrangement of **10** led to almost quantitative formation of the iminium product **10i** inside the host cavity at pD 8.00 (Figure 10).<sup>48</sup> That is, subsequent hydrolysis of encapsulated **10i** was slow compared to the initial rearrangement step and therefore could be monitored over time. The decay of  $[10\text{iC Ga}_4\text{L}_6]^{11-}$  displayed clean first-order kinetics, and a rate of hydrolysis could be obtained (Figure 11).

Other studies by Raymond and co-workers have established that negatively charged molecules cannot enter the host cavity, even transiently, due to strong electrostatic repulsion with the highly negatively charged host structure.<sup>49</sup> Hydrolysis of iminium cations takes place at neutral pH but can also be catalyzed by hydroxide ions.<sup>50</sup> If hydrolysis of **10i** proceeds exclusively inside the protective host cavity, which prevents hydroxide ions from entering, the rate of hydrolysis should be independent of hydroxide concentration. The only nucleophile that can potentially enter the inner space is water, and its concentration remains constant when it is used as the solvent. If, however, iminium dissociation precedes hydrolysis, a pH dependence is anticipated; outside of the shielded cavity, the iminium ion can be attacked by the hydroxide nucleophile.

A series of kinetic runs was performed in buffered solutions over a pD range from 6.5 to 12.8, and the data are summarized

(47) “Empty” cavity in this case refers to the host assembly, incorporating 1 equiv of  $\text{NMe}_4^+$ .  $\text{NMe}_4^+$  is a very weakly binding guest molecule and can easily be replaced by the entering enammonium substrates.

(48) For several of the other substrates **2–9**, iminium formation was also detected, but product **10i** is unique in that its rate of formation is substantially greater than its rate of displacement from the cavity. Presumably, **10i** has a higher binding constant for the cavity interior compared to those of the other iminium intermediates, which results in a longer lifetime.

(49) Leung, D.; Bergman, R. G.; Raymond, K. N., unpublished results.

(50) Hine, J.; Evangelista, R. A. *J. Am. Chem. Soc.* **1980**, *102*, 1649–1655.

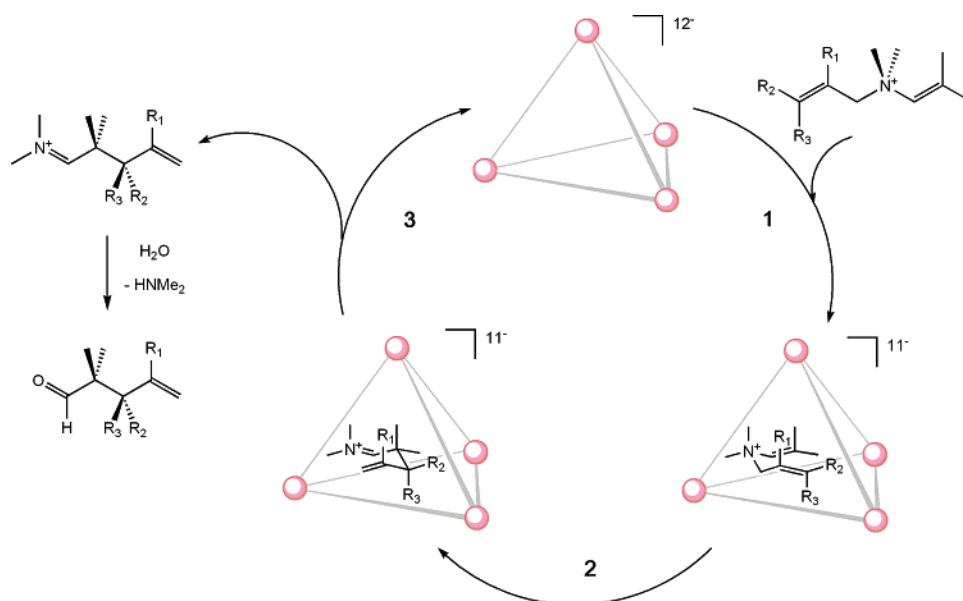


**Figure 9.** Proposed catalytic cycle for the cationic 3-aza Cope rearrangement.

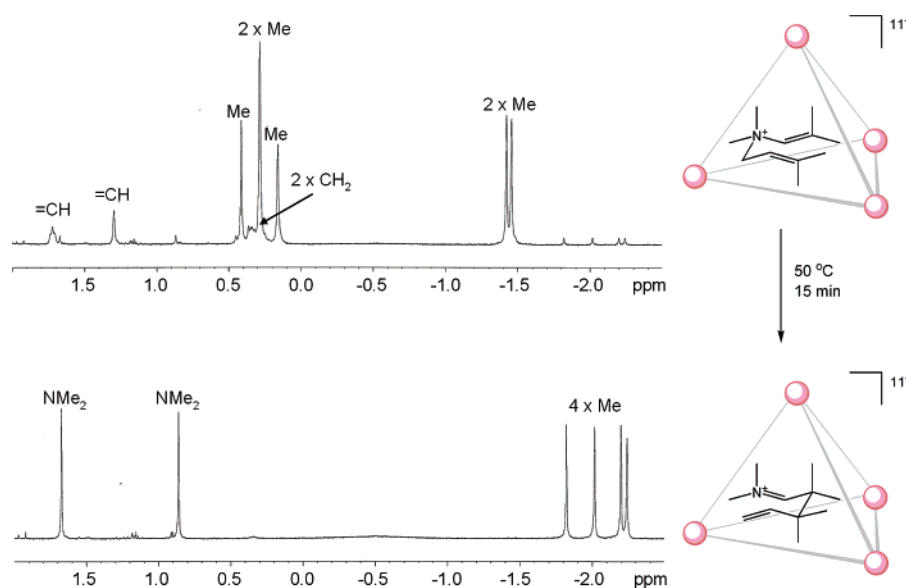


**Figure 10.** Rearrangement of  $[10\text{C}_{\text{Ga}_4\text{L}_6}]^{11-}$  leads to almost quantitative formation of the encapsulated iminium product  $[10\text{iC}_{\text{Ga}_4\text{L}_6}]^{11-}$ .

in Figure 12. In the neutral pD range (pD 6–8), the rates of hydrolysis are almost constant; presumably in this range water acts as the nucleophile. At increasing pD, however, a dependence on hydroxide concentration is observed up to a pD of about 11, at which point the system seems to reach saturation.

The linear first-order dependence on hydroxide concentration in the pD 9–10.5 range supports a mechanistic model which envisions reversible iminium egression before hydrolysis. The rate at saturation implies that iminium dissociation becomes rate limiting, because hydrolysis becomes faster than re-encapsulation. One surprising aspect of this rationale is that the rate of guest egression did not compare very well to previously reported rates of exchange for guest molecules of similar size and shape.<sup>51</sup> For example, the rate constant for guest exchange at 50 °C for  $\text{NMe}_2\text{Pr}_2^+$  is  $k_{323}(\text{NMe}_2\text{Pr}_2^+) = 1020 \text{ s}^{-1}$ , which is about 500 000 times faster than the rate constant reached at saturation

for **10i**,  $k_{323}(\mathbf{10i}) = 0.002 \text{ s}^{-1}$ . Prior kinetic experiments also demonstrated that rates of guest exchange were sensitive to the concentration of “innocent” counterions, cations that did not actively participate in guest exchange, such as  $\text{NMe}_4^+$ . Throughout the previous experiments, the concentration of  $\text{NMe}_4^+$  was held constant (6 equiv used in all experiments).

To elucidate the role of  $\text{NMe}_4^+$  in the rearrangement reaction and iminium hydrolysis, variable  $[\text{NMe}_4^+]$  kinetics were conducted at high pD (12.64) and constant ionic strength (0.5 M, adjusted with KCl). The kinetics revealed a significant dependence of iminium hydrolysis on  $[\text{NMe}_4^+]$  concentration (Figure 13). Increased  $[\text{NMe}_4^+]$  concentration led to faster hydrolysis, and a first-order dependence on  $[\text{NMe}_4^+]$  was observed. At higher concentrations of  $[\text{NMe}_4^+]$ , saturation behavior was again observed.

The dependence of  $k_{\text{obs}}$  on  $[\text{NMe}_4^+]$  can be interpreted in two ways. If we assume an  $\text{S}_{\text{N}}2$ -type bimolecular pathway for guest exchange, added  $\text{NMe}_4^+$  might assist guest displacement

(51) Davis, A. V.; Fiedler, D.; Seeber, G.; Zahl, A.; van Eldik, R.; Raymond, K. N. *J. Am. Chem. Soc.* **2006**, *128*, 1324–1333.

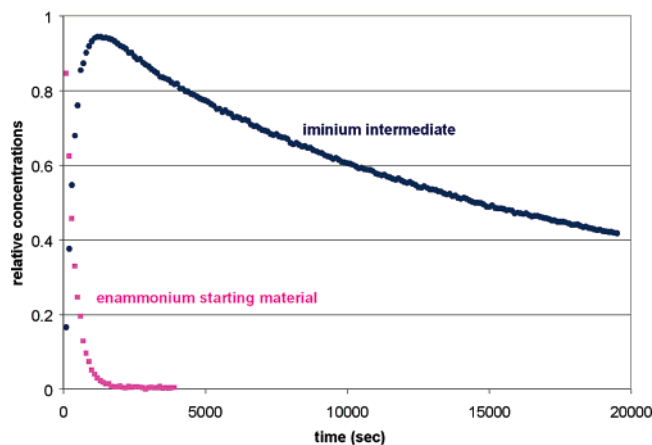


**Figure 11.** Disappearance of starting material  $[10\text{C}\text{Ga}_4\text{L}_6]^{11-}$  (pink ■) is accompanied by formation of  $[10\text{iC}\text{Ga}_4\text{L}_6]^{11-}$ . Hydrolysis of  $[10\text{iC}\text{Ga}_4\text{L}_6]^{11-}$  (blue ●) is slow and can be monitored over time. Concentrations are measured relative to an internal standard.

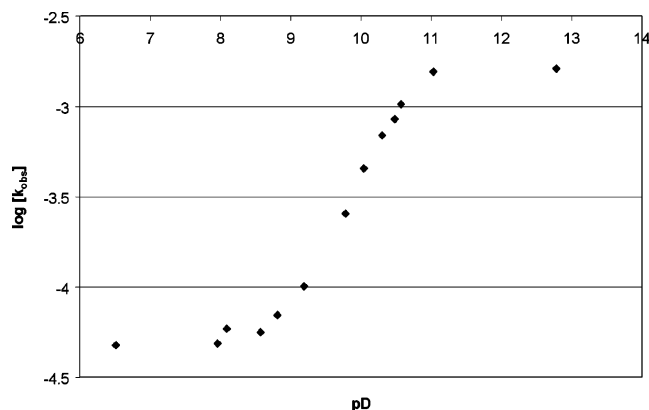


**Figure 12.** Plot of  $\log[k_{\text{obs}}]$  versus pD reveals a dependence on hydroxide concentration for the hydrolysis reaction.

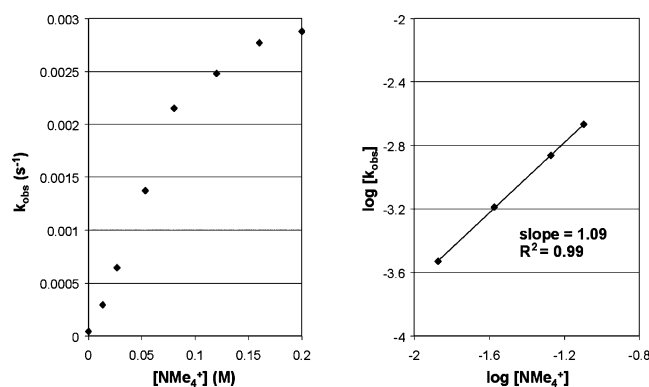


**Figure 13.** Kinetics with variable concentrations of  $\text{NMe}_4^+$  reveal a first-order dependence of the rate of iminium hydrolysis on  $\text{NMe}_4^+$  concentration.

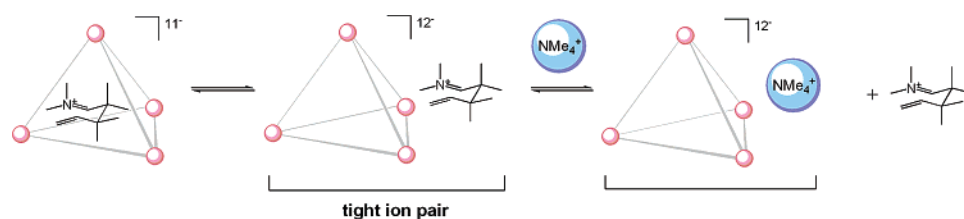


**Figure 14.** Tight ion pairing might be responsible for the dependence of iminium hydrolysis on the counterion  $\text{NMe}_4^+$ .

from the cavity interior, thus accelerating release of the iminium cation into the surrounding basic solution. However,  $\text{NMe}_4^+$  is an extremely weakly binding guest, making this explanation unlikely. In contrast, calorimetric studies have suggested a significant interaction of  $\text{NMe}_4^+$  with the assembly exterior;<sup>52</sup> in fact, the affinity of  $\text{NMe}_4^+$  is higher for exterior than interior binding sites ( $K_{\text{ext}} = 50 \text{ M}^{-1}$ ,  $K_{\text{int}} = 33 \text{ M}^{-1}$ ). This exterior interaction implies the intermediacy of a tight ion pair of the tetrahedral host with the iminium cation, as illustrated in Figure 14. We suggest that, in the tight ion pair, **10i** is closely associated with the anionic host, not allowing hydroxide to attack the iminium due to electrostatic repulsion. Only when **10i** is released into solution can hydroxide-catalyzed hydrolysis take place.

To determine which pathway was operating, the rate dependence on  $[\text{NBu}_4^+]$  was studied. The tetrabutylammonium cation is too large to fit into the cavity interior and therefore cannot displace a guest molecule from that location. Exterior counterion displacement, in contrast, is viable, since calorimetric studies indicate a strong exterior interaction of tetrabutylammonium with the metal–ligand assembly.<sup>52</sup> As was the case with  $\text{NMe}_4^+$ , increasing concentrations of  $\text{NBu}_4^+$  led to faster rates of hydrolysis, and a first order dependence on  $[\text{NBu}_4^+]$  was observed (see Supporting Information).<sup>53</sup> With this information, the mechanistic model illustrated in Figure 14, which proposes the intermediacy of a tight ion pair between the exiting iminium cation and the assembly exterior, becomes more persuasive.

Additional proof for an intermediate that contains iminium **10i** ion paired to the assembly exterior comes from a trapping experiment with  $\text{NEt}_4^+$ , which is a very strongly binding guest molecule that displaces almost all other ammonium cations. Under the conditions of slowest iminium hydrolysis (pD 6.5 and no added counterions), about 1.5 equiv of  $\text{NEt}_4^+$  was added to a solution of  $\text{K}_{11}[\mathbf{10iC}\text{Ga}_4\text{L}_6]$ . An exchange reaction took place within minutes and could be monitored by  $^1\text{H}$  NMR spectroscopy.  $\text{NEt}_4^+$  now occupies the cavity interior, and two new broad resonances at 2.43 and 0.78 ppm emerge. Integration of these peaks suggests that the resonance at 2.43 ppm corresponds to the  $\text{NMe}_2^+$  methyl groups, whereas the broad signal at 0.78 ppm accounts for the other four methyl groups of **10i** (see Supporting Information). The slight upfield shift of those resonances and their broadness imply a tight ion-pairing interaction with the assembly exterior. As anticipated, slow hydrolysis of **10i** takes place, and the resonances of the ion-paired exterior iminium ion decay over time.

These observations of strong external interactions of the exiting guest molecule with the host structure are further substantiated by the findings of Leung et al.<sup>54</sup> To determine the rate for guest passage, several large phosphine ligands were used to trap a cationic iridium guest species upon egression from the cavity. Surprisingly, a neutral phosphine could trap the iridium complex much faster than a trianionic phosphine. When



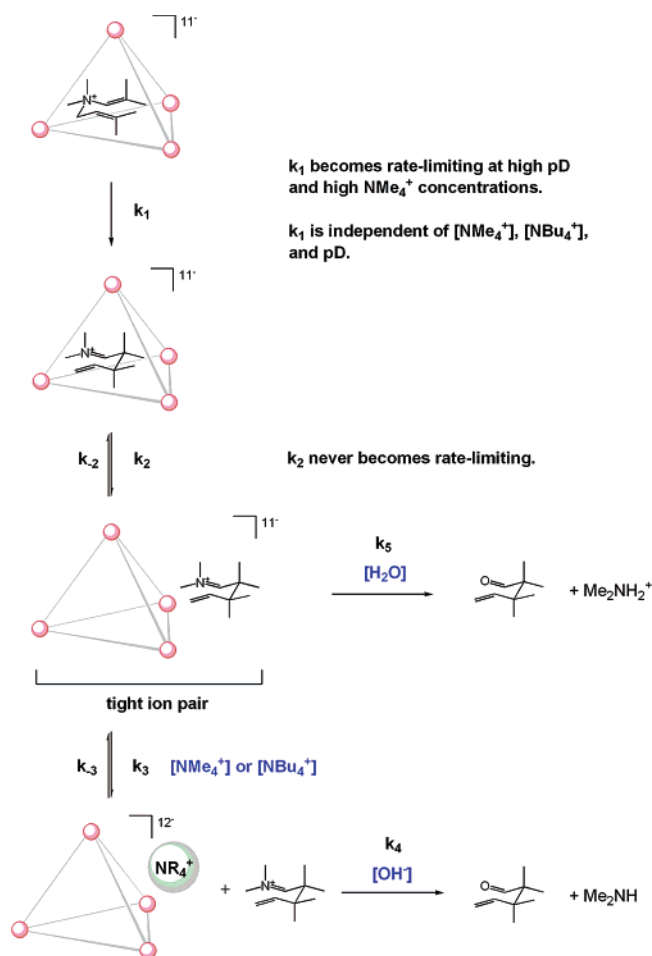


**Figure 15.** Overall proposed mechanism of iminium hydrolysis.

considering the possibility of an intermediate tight ion pair of the cationic iridium complex with the host exterior, Leung et al. were able to rationalize their findings: due to electrostatic repulsion, the anionic phosphine cannot come close enough to the iridium center when engaged in the ion pair, therefore slowing the apparent rate of trapping compared to the neutral phosphine trap.

The overall proposed mechanism is illustrated in Figure 15: the encapsulated enammonium substrate **10** rearranges inside the cavity interior to the iminium cation **10i** ( $k_1$ ). The rearrangement step is, as anticipated, independent of pD and  $\text{NMe}_4^+$  concentration (see Supporting Information). The product **10i** can reversibly dissociate from the interior to the assembly exterior, where it is tightly ion paired ( $k_2$ ). In the presence of the counterions  $\text{NMe}_4^+$  and  $\text{NBu}_4^+$ , which have significant affinity for the assembly exterior, **10i** can be displaced from the exterior and released into the surrounding solution ( $k_3$ ). Once **10i** is dissociated from the highly negatively charged cage, hydroxide can attack the iminium ion, catalyzing its hydrolysis to the corresponding aldehyde ( $k_4$ ). In the absence of  $\text{NMe}_4^+$  or  $\text{NBu}_4^+$ , breakup of the tight ion pair is very slow; in this case, the slow

(52) Michels, M.; Raymond, K. N., unpublished results.

(53) The strong exterior interactions of  $\text{NBu}_4^+$  with the supramolecular host are also evidenced by the altered solubility properties of the host–guest assembly. Addition of more than 2 equiv of  $\text{NBu}_4^+$  led to immediate precipitation of the assembly, presumably due to coordination of the ions to the exterior. The experimentally accessible concentration range for  $\text{NBu}_4^+$  was therefore limited.

(54) Leung, D. H.; Bergman, R. G.; Raymond, K. N. *J. Am. Chem. Soc.*, in press.

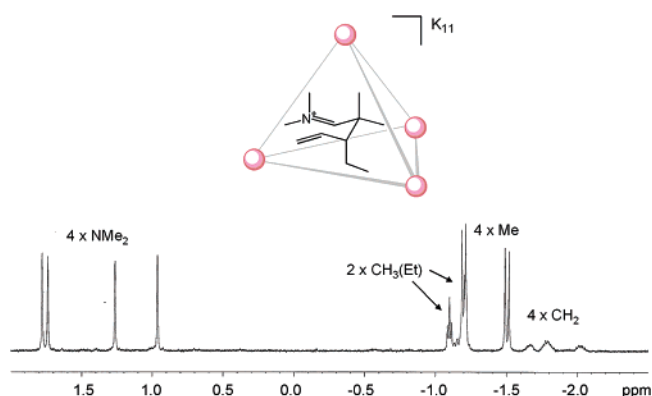


**Figure 16.** Rearrangement of  $\text{K}_{11}[\text{3C-Ga}_4\text{L}_6]$  (shown) and  $\text{K}_{11}[\text{4C-Ga}_4\text{L}_6]$  (not shown) leads to almost quantitative formation of the corresponding encapsulated iminium species. Since the iminium cation is chiral, the formation of two diastereomers is observed.

disappearance of **10i** is observed due to a background reaction. This background reaction is the water-mediated hydrolysis of **10i**, since water, as a neutral nucleophile, can approach and intercept the ion-paired iminium cation ( $k_5$ ).

This argument is supported by the fact that the rates of hydrolysis for  $\text{K}_{11}[\text{10iC-Ga}_4\text{L}_6]$  are independent of pD, in the absence of exterior counterions  $\text{NMe}_4^+$  and  $\text{NBu}_4^+$ . The observed rate constants for the disappearance of **10i** are essentially identical at pD 6.5 and 12.8 and correspond to the background reaction rate rate  $k_5$ . Even at elevated pD, hydroxide cannot approach the ion-paired iminium ion and hydrolysis relies on the neutral nucleophile water.

**Chiral Induction in Sigmatropic Rearrangements.** In the absence of strongly binding counterions, the iminium intermediate **10i** had a remarkably long lifetime inside (and bound externally to) the supramolecular host ( $t_{1/2} \approx 4$  h). A similar phenomenon was observed for the other substrates, **1–8**. In the absence of added  $\text{NMe}_4^+$ , the lifetime of the iminium intermediates was increased, and the formation of the iminium intermediates was fast compared to their rates of hydrolysis (except for **9**), allowing for their detection by  $^1\text{H}$  NMR spectroscopy.<sup>55</sup> Since the rearrangement of prochiral substrates **3–8** led to chiral iminium products, the formation of two diastereomeric host–guest complexes was the result. A representative  $^1\text{H}$  NMR spectrum of the rearranged products of  $\text{K}_{11}[\text{3C-Ga}_4\text{L}_6]$  is shown in Figure 16. The resonances for the two diastereomeric guests are well resolved and allow for the quantification of the diastereomeric excesses in these reactions.

Unfortunately, the degree of stereoselectivity in these reactions is very low, and only for the rearrangement of  $\text{K}_{11}[\text{8C-Ga}_4\text{L}_6]$  was a notable discrimination between the two diastereomeric transition states observed: one of the iminium enantiomers is formed with a diastereomeric excess of  $\sim 20\%$ .

These results imply that, in principle, the resolved host structure could serve as a stereoselective reaction vessel for pericyclic reactions. The realization of catalytic enantioselective pericyclic reactions has proven to be a challenge. In particular, no good method for induction of stereoselectivity exists for substrates that do not contain any coordinating groups (func-

(55) In previous experiments, 6 equiv of  $\text{NMe}_4^+$  was present, resulting in a more transient nature of the iminium products **2i–8i**. We believe that  $\text{NMe}_4^+$  is able to displace the iminium products from the cavity interior; concentration of the weakly bound **2i–8i** can only build up in the absence of competing guest molecules.

tional groups with which the substrate can coordinate to a chiral Lewis acid).<sup>43,56,57</sup> The approach employed here thus constitutes an attractive alternative: instead of employing complicated chiral auxiliaries, chirality in these reactions is envisioned to be transmitted by the chiral host environment. This system, however, still needs to be optimized, and structural features that will lead to higher degrees of recognition and stereoselectivity need to be identified and introduced into the structures of either host or guest.

## Conclusion

Overall, our findings emphasize the ability of molecular container compounds to provide a well-defined microenvironment which can be utilized for the catalysis of unimolecular rearrangements. By binding the substrates in reactive conformations, as evidenced by kinetic, activation parameter, and quantitative NOE studies, the host assembly accelerates the rates of rearrangement by up to 3 orders of magnitude. The cavity-catalyzed rearrangement is followed by product release from the cavity interior to an exterior binding site, where it can then be hydrolyzed, and this hydrolysis step generates catalytic turnover. With this, the large potential of supramolecular assemblies as synthetically useful tools in organic chemistry becomes apparent, and we can be certain that, with the multitude of available supramolecular structures, many transformations susceptible to supramolecular catalysis are to be discovered.

## Experimental Section

**General Considerations.** All reagents were obtained from commercial suppliers and used without further purification unless stated otherwise. Anhydrous solvents were dried over activated alumina.  $K_6$ -( $NMe_4$ )<sub>5</sub>[ $NMe_4$ C $Ga_4L_6$ ],  $K_{12}$ [ $Ga_4L_6$ ],  $Na_{12}$ [ $Ga_4L_6$ ], and  $N,N$ -dimethylisobutylamine were prepared according to the published procedures.<sup>58,59</sup> NMR spectra were obtained on Bruker Avance AV 400 or DRX 500 MHz spectrometers. <sup>1</sup>H chemical shifts are reported as  $\delta$  in ppm relative to residual protonated solvent resonances; <sup>13</sup>C chemical shifts are measured relative to solvent resonances and reported as  $\delta$  in ppm. Coupling constants are reported in hertz. IR spectra were recorded on an Avatar 370 FT-IR instrument. Elemental analyses were performed by the Microanalytical Laboratory in the College of Chemistry at the University of California, Berkeley, and amounts of solvent contained in the analyses were confirmed by <sup>1</sup>H NMR spectroscopy. Electrospray mass spectra were recorded on a triple-quadrupole VG Quattro mass spectrometer in the Mass Spectrometry Laboratory in the College of Chemistry at the University of California, Berkeley. FAB spectra were recorded at the University of California, Berkeley, Mass Spectrometry facility; the symbol  $N^+$  denotes the parent ion of the enammonium cation.

**General Procedure for Tosylation Reactions.** This is a modified literature procedure:<sup>60</sup> in a 500 mL Schlenk flask, 15.0 mM of the appropriate allyl alcohol was combined with 80 mL of dry and degassed THF, and the solution was cooled to  $-78$  °C. To this solution was added  $n$ -BuLi (9.34 mL, 15.0 mM, 1.6 M in hexanes). Tosyl chloride (2.86 g, 15.0 mM) was added in a single portion, and the homogeneous solution was put in the freezer at  $-80$  °C for 2 days. The reaction was worked up by diluting the reaction mixture at  $-78$  °C with 150 mL of

cold petroleum ether. The organic phase was washed with  $2 \times 50$  mL of 50% saturated aqueous  $NaHCO_3$  and  $1 \times 50$  mL of saturated aqueous  $NaHCO_3$ . The aqueous layers were combined and extracted with  $1 \times 50$  mL of petroleum ether, and the combined organic layers were dried over  $K_2CO_3$ . After filtration, the volatile materials were removed by rotary evaporation, leaving behind the allyl tosylates as colorless to pale yellow oils in quantitative yields. The tosylates were characterized by <sup>1</sup>H NMR only and used without further purification. The tosylates can be stored in a benzene matrix at  $-80$  °C for several weeks.

**Data for Allyl Tosylates, Prepared As Described Above. *cis*-2-Pentenyl Tosylate.** <sup>1</sup>H NMR (500 MHz,  $CDCl_3$ ):  $\delta$  7.80 (d, <sup>3</sup> $J$  = 8.0 Hz, 2H, OTs), 7.34 (d, <sup>3</sup> $J$  = 8.0 Hz, 2H, OTs), 5.66 (m, 1H, =CH), 5.41 (m, 1H, =CH), 4.60 (d, <sup>3</sup> $J$  = 7.5 Hz, 2H,  $OCH_2$ ), 2.45 (s, 3H, OTs), 1.99 (quint., <sup>3</sup> $J$  = 7.5 Hz, 2H,  $CH_2$ ), 0.93 (t, <sup>3</sup> $J$  = 7.5 Hz, 3H,  $CH_3$ ).

***trans*-2-Hexenyl Tosylate.** <sup>1</sup>H NMR (500 MHz,  $CDCl_3$ ):  $\delta$  7.79 (d, <sup>3</sup> $J$  = 8.0 Hz, 2H, OTs), 7.34 (d, <sup>3</sup> $J$  = 8.0 Hz, 2H, OTs), 5.74 (dt, <sup>3</sup> $J$  = 15.5 Hz, <sup>3</sup> $J$  = 6.5 Hz, 1H, =CH), 5.45 (dt, <sup>3</sup> $J$  = 15.5 Hz, <sup>3</sup> $J$  = 7.0 Hz, 1H, =CH), 4.49 (d, <sup>3</sup> $J$  = 7.0 Hz, 2H,  $OCH_2$ ), 2.44 (s, 3H, OTs), 1.97 (m, 2H,  $CH_2$ ), 1.36 (sext., <sup>3</sup> $J$  = 7.5 Hz, 2H,  $CH_2$ ), 0.83 (t, <sup>3</sup> $J$  = 7.5 Hz, 3H,  $CH_3$ ).

***cis*-2-Hexenyl Tosylate.** <sup>1</sup>H NMR (500 MHz,  $CDCl_3$ ):  $\delta$  7.79 (d, <sup>3</sup> $J$  = 8.2 Hz, 2H, OTs), 7.34 (d, <sup>3</sup> $J$  = 8.0 Hz, 2H, OTs), 5.66 (dt, <sup>3</sup> $J$  = 10.9 Hz, <sup>3</sup> $J$  = 7.6 Hz, 1H, =CH), 5.45 (dtt, <sup>3</sup> $J$  = 10.9 Hz, <sup>3</sup> $J$  = 7.1 Hz, <sup>4</sup> $J$  = 1.4 Hz, 1H, =CH), 4.59 (d, <sup>3</sup> $J$  = 7.1 Hz, 2H,  $OCH_2$ ), 2.44 (s, 3H, OTs), 1.94 (qd, <sup>3</sup> $J$  = 7.5 Hz, <sup>4</sup> $J$  = 1.3 Hz, 2H,  $CH_2$ ), 1.32 (sext., <sup>3</sup> $J$  = 7.4 Hz, 2H,  $CH_2$ ), 0.83 (t, <sup>3</sup> $J$  = 7.4 Hz, 3H,  $CH_3$ ).

**4-Methyl-2-*trans*-pentenyl Tosylate.** <sup>1</sup>H NMR (500 MHz,  $C_6D_6$ ):  $\delta$  7.76 (d, <sup>3</sup> $J$  = 8.2 Hz, 2H, OTs), 6.67 (d, <sup>3</sup> $J$  = 8.0 Hz, 2H, OTs), 5.32 (dd, <sup>3</sup> $J$  = 15.4 Hz, <sup>3</sup> $J$  = 6.5 Hz, 1H, =CH), 5.18 (dtd, <sup>3</sup> $J$  = 15.4 Hz, <sup>3</sup> $J$  = 6.5 Hz, <sup>4</sup> $J$  = 1.2 Hz, 1H, =CH), 4.32 (d, <sup>3</sup> $J$  = 6.6 Hz, 2H,  $OCH_2$ ), 1.90 (sext., <sup>3</sup> $J$  = 6.7 Hz, 1H, *i*-Pr), 1.82 (s, 3H, OTs), 0.70 (d, <sup>3</sup> $J$  = 6.8 Hz, 6H, *i*-Pr).

***trans*-2-Heptenyl Tosylate.** <sup>1</sup>H NMR (500 MHz,  $CDCl_3$ ):  $\delta$  7.79 (d, <sup>3</sup> $J$  = 8.3 Hz, 2H, OTs), 7.33 (d, <sup>3</sup> $J$  = 8.1 Hz, 2H, OTs), 5.74 (dt, <sup>3</sup> $J$  = 15.3 Hz, <sup>3</sup> $J$  = 6.7 Hz, 1H, =CH), 5.44 (dtt, <sup>3</sup> $J$  = 15.3 Hz, <sup>3</sup> $J$  = 6.7 Hz, <sup>4</sup> $J$  = 1.4 Hz, 1H, =CH), 4.49 (d, <sup>3</sup> $J$  = 6.7 Hz, 2H,  $OCH_2$ ), 2.44 (s, 3H, OTs), 1.99 (m, 2H,  $CH_2$ ), 1.27 (m, 4H,  $CH_2$ ), 0.86 (t, <sup>3</sup> $J$  = 7.0 Hz, 3H,  $CH_3$ ).

***trans*-3-(Trimethylsilyl)allyl Tosylate.** <sup>1</sup>H NMR (500 MHz,  $CDCl_3$ ):  $\delta$  7.80 (d, <sup>3</sup> $J$  = 8.3 Hz, 2H, OTs), 7.34 (d, <sup>3</sup> $J$  = 8.0 Hz, 2H, OTs), 5.97–5.86 (m, 2H, =CH), 4.54 (d, <sup>3</sup> $J$  = 3.9 Hz, 2H,  $OCH_2$ ), 2.45 (s, 3H, OTs), 0.02 (s, 9H, TMS).

**General Procedure for Alkylation Reactions.** This is a modified literature procedure:<sup>38</sup> under a moisture-free atmosphere, a cooled solution (0 °C) of  $N,N$ -dimethylisobutylamine (500  $\mu$ L, 3.76 mmol) in 5 mL of dry acetonitrile was combined with a cooled solution of the appropriate allyl or propargyl bromide/tosylate (4.14 mmol) in 5 mL of acetonitrile via cannula. The reaction mixture was stirred at 0 °C for 48 h. All volatile materials were removed under reduced pressure, leading to sticky, oily residues. The residues were washed with  $5 \times 20$  mL of dry  $Et_2O$ , yielding the analytically pure products.

**Data for Enammonium Salts, Prepared As Described Above. [ $NMe_2$ (allyl)( $CH=C(CH_3)_2$ )]<sup>+</sup> $Br^-$  (1-Br).** The product was isolated as a very hygroscopic white powder in 94% yield (778 mg, 3.53 mmol). <sup>1</sup>H NMR (500 MHz,  $CDCl_3$ ):  $\delta$  5.95 (s, br, 1H, =CH), 5.84 (dtd, <sup>3</sup> $J$  = 16.9 Hz, <sup>3</sup> $J$  = 9.9 Hz, <sup>3</sup> $J$  = 7.1 Hz, 1H, =CH), 5.75 (dd, <sup>3</sup> $J$  = 16.9 Hz, <sup>2</sup> $J$  = 1.2 Hz, 1H, = $CH_2$ ), 5.56 (dd, <sup>3</sup> $J$  = 9.9 Hz, <sup>2</sup> $J$  = 1.3 Hz, 1H, = $CH_2$ ), 4.50 (d, <sup>3</sup> $J$  = 7.0 Hz, 2H,  $CH_2$ ), 3.50 (s, 6H,  $N(CH_3)_2$ ), 1.92 (d, <sup>4</sup> $J$  = 1.3 Hz, 3H,  $CH_3$ ), 1.74 (d, <sup>4</sup> $J$  = 1.3 Hz, 3H,  $CH_3$ ). <sup>13</sup>C{<sup>1</sup>H} (125.8 MHz,  $CDCl_3$ ):  $\delta$  135.2 (=CH), 129.1 (=CH), 128.5 ( $C_{quat}$ ), 124.8 (=CH<sub>2</sub>), 69.3 ( $CH_2$ ), 54.1 ( $N(CH_3)_2$ ), 25.3 ( $CH_3$ ), 19.1 ( $CH_3$ ). IR (neat):  $\nu$  = 3065, 3032, 3013, 2934, 1473, 1462, 1444, 1426, 1404, 1381, 1086, 1023  $cm^{-1}$ . LRFAB-MS (+):  $m/z$  140 [ $N^+$ ]. Anal. Calcd for  $C_9H_{18}BrN$ : C, 49.10; H, 8.24; N, 6.36. Found: C, 48.88; H, 8.39; N, 6.12.

- (56) Hiersemann, M.; Abraham, L. *Eur. J. Org. Chem.* **2002**, 1461–1471.  
 (57) Abraham, L.; Czerwonka, R.; Hiersemann, M. *Angew. Chem., Int. Ed.* **2001**, *40*, 4700–4703.  
 (58) Caulder, D. L.; Powers, R. E.; Parac, T. N.; Raymond, K. N. *Angew. Chem., Int. Ed.* **1998**, *37*, 1840–1843.  
 (59) Ellenberger, M. R.; Dixon, D. A.; Farneth, W. E. *J. Am. Chem. Soc.* **1981**, *103*, 5377–5382.  
 (60) Barta, N. S.; Cook, G. R.; Landis, M. S.; Stille, J. R. *J. Org. Chem.* **1992**, *57*, 7188–7194.

**[NMe<sub>2</sub>(methallyl)(CH=C(CH<sub>3</sub>)<sub>2</sub>)]<sup>+</sup>Br<sup>-</sup> (2-Br).** The product was isolated as a very hygroscopic white powder in 91% yield (801 mg, 3.42 mmol). <sup>1</sup>H NMR (500 MHz, CDCl<sub>3</sub>): δ 5.98 (s, br, 1H, =CH), 5.47 (d, <sup>2</sup>J = 1.3 Hz, 1H, =CH), 5.30 (d, <sup>2</sup>J = 1.3 Hz, 1H, =CH), 4.43 (s, 2H, CH<sub>2</sub>), 3.48 (s, 6H, N(CH<sub>3</sub>)<sub>2</sub>), 1.91 (d, <sup>4</sup>J = 1.4 Hz, 3H, CH<sub>3</sub>), 1.77 (s, 3H, CH<sub>3</sub>), 1.71 (d, <sup>4</sup>J = 1.4 Hz, 3H, CH<sub>3</sub>). <sup>13</sup>C{<sup>1</sup>H} (125.8 MHz, CDCl<sub>3</sub>): δ 134.3 (=CH), 133.4 (=CH), 129.5 (C<sub>quart</sub>), 127.2 (=CH), 72.2 (CH<sub>2</sub>), 54.5 (N(CH<sub>3</sub>)<sub>2</sub>), 25.3 (CH<sub>3</sub>), 22.9 (CH<sub>3</sub>), 19.1 (CH<sub>3</sub>). IR (neat): ν = 3010, 2971, 2943, 2736, 1643, 1468, 1440, 1418, 1372, 1085, 1006 cm<sup>-1</sup>. LRFAB-MS (+): *m/z* 154 [N<sup>+</sup>]. Anal. Calcd for C<sub>10</sub>H<sub>20</sub>BrN: C, 51.29; H, 8.61; N, 5.98. Found: C, 51.02; H, 8.83; N, 5.80.

**[NMe<sub>2</sub>(*trans*-2-pentenyl)(CH=C(CH<sub>3</sub>)<sub>2</sub>)]<sup>+</sup>Br<sup>-</sup> (3-Br).** The product was isolated as a hygroscopic colorless oil in 95% yield (887 mg, 3.57 mmol). <sup>1</sup>H NMR (500 MHz, CDCl<sub>3</sub>): δ 6.20 (dt, <sup>3</sup>J = 15.3 Hz, <sup>3</sup>J = 6.4 Hz, 1H, =CH), 5.87 (s, br, 1H, =CH), 5.40 (dt, <sup>3</sup>J = 15.3 Hz, <sup>3</sup>J = 7.6 Hz, 1H, =CH), 4.39 (d, <sup>3</sup>J = 7.4 Hz, 2H, CH<sub>2</sub>), 3.44 (s, 6H, N(CH<sub>3</sub>)<sub>2</sub>), 2.02 (quint., <sup>3</sup>J = 7.2 Hz, 2H, CH<sub>2</sub>), 1.90 (d, <sup>4</sup>J = 1.3 Hz, 3H, CH<sub>3</sub>), 1.73 (d, <sup>4</sup>J = 1.3 Hz, 3H, CH<sub>3</sub>). <sup>13</sup>C{<sup>1</sup>H} (125.8 MHz, CDCl<sub>3</sub>): δ 148.1 (=CH), 134.9 (=CH), 128.5 (C<sub>quart</sub>), 115.3 (=CH), 69.2 (CH<sub>2</sub>), 53.7 (N(CH<sub>3</sub>)<sub>2</sub>), 25.5 (CH<sub>3</sub>), 25.3 (CH<sub>2</sub>), 19.1 (CH<sub>3</sub>), 12.5 (CH<sub>3</sub>). LRFAB-MS (+): *m/z* 168 [N<sup>+</sup>]. IR (neat): ν = 3010, 2963, 2935, 2874, 1665, 1462, 1453, 1375, 1086 cm<sup>-1</sup>. Anal. Calcd for C<sub>11</sub>H<sub>22</sub>BrN: C, 53.23; H, 8.93; N, 5.64. Found: C, 52.88; H, 9.23; N, 5.73.

**[NMe<sub>2</sub>(*cis*-2-pentenyl)(CH=C(CH<sub>3</sub>)<sub>2</sub>)]<sup>+</sup>OTs<sup>-</sup> (4-OTs).** The product was isolated as a white hygroscopic powder in 94% yield (887 mg, 3.57 mmol). <sup>1</sup>H NMR (500 MHz, CDCl<sub>3</sub>): δ 7.73 (d, <sup>3</sup>J = 8.1 Hz, 2H, OTs), 7.10 (d, <sup>3</sup>J = 7.9 Hz, 2H, OTs), 5.92 (dt, <sup>3</sup>J = 10.9 Hz, <sup>3</sup>J = 7.7 Hz, 1H, =CH), 5.83 (s, br, 1H, =CH), 5.39 (dt, <sup>3</sup>J = 10.9 Hz, <sup>3</sup>J = 7.8 Hz, 1H, =CH), 4.31 (d, <sup>3</sup>J = 7.7 Hz, 2H, CH<sub>2</sub>), 3.44 (s, 6H, N(CH<sub>3</sub>)<sub>2</sub>), 2.30 (s, 3H, OTs), 2.02 (dq, <sup>3</sup>J = 7.6 Hz, <sup>4</sup>J = 1.3 Hz, 2H, CH<sub>2</sub>), 1.91 (d, <sup>4</sup>J = 1.3 Hz, 3H, CH<sub>3</sub>), 1.74 (d, <sup>4</sup>J = 1.3 Hz, 3H, CH<sub>3</sub>), 0.91 (t, <sup>3</sup>J = 7.5 Hz, 3H, CH<sub>3</sub>). <sup>13</sup>C{<sup>1</sup>H} (125.8 MHz, CDCl<sub>3</sub>): δ 145.0 (=CH), 143.9 (OTs), 139.0 (OTs), 134.9 (=CH), 128.7 (C<sub>quart</sub>), 128.5 (OTs), 125.8 (OTs), 115.2 (=CH), 63.9 (CH<sub>2</sub>), 53.9 (N(CH<sub>3</sub>)<sub>2</sub>), 25.5 (OTs), 21.2, 21.1, 18.9, 13.5 (CH<sub>3</sub> and CH<sub>2</sub>). IR (neat): ν = 3028, 2966, 2934, 2872, 1483, 1461, 1205, 1184, 1119, 1032, 1010 cm<sup>-1</sup>. LRFAB-MS (+): *m/z* 168 [N<sup>+</sup>]. Anal. Calcd for C<sub>18</sub>H<sub>29</sub>NO<sub>3</sub>S: C, 63.68; H, 8.61; N, 4.13. Found: C, 63.50; H, 8.79; N, 4.19.

**[NMe<sub>2</sub>(*trans*-2-hexenyl)(CH=C(CH<sub>3</sub>)<sub>2</sub>)]<sup>+</sup>OTs<sup>-</sup> (5-OTs).** The product was isolated as a hygroscopic colorless oil in 88% yield (1.12 g, 3.31 mmol) which solidified upon standing in the freezer at -30 °C. <sup>1</sup>H NMR (500 MHz, CDCl<sub>3</sub>): δ 7.73 (d, <sup>3</sup>J = 8.1 Hz, 2H, OTs), 7.11 (d, <sup>3</sup>J = 7.9 Hz, 2H, OTs), 6.06 (dt, <sup>3</sup>J = 15.3 Hz, <sup>3</sup>J = 6.9 Hz, 1H, =CH), 5.81 (s, br, 1H, =CH), 5.40 (dt, <sup>3</sup>J = 15.3 Hz, <sup>3</sup>J = 7.4 Hz, 1H, =CH), 4.23 (d, <sup>3</sup>J = 7.4 Hz, 2H, CH<sub>2</sub>), 3.39 (s, 6H, N(CH<sub>3</sub>)<sub>2</sub>), 2.30 (s, 3H, OTs), 2.02 (quart., <sup>3</sup>J = 7.0 Hz, 2H, CH<sub>2</sub>), 1.90 (d, <sup>4</sup>J = 1.4 Hz, 3H, CH<sub>3</sub>), 1.74 (d, <sup>4</sup>J = 1.4 Hz, 3H, CH<sub>3</sub>), 1.36 (sext., <sup>3</sup>J = 7.4 Hz, 2H, CH<sub>2</sub>), 0.85 (t, <sup>3</sup>J = 7.3 Hz, 3H, CH<sub>3</sub>) ppm. <sup>13</sup>C{<sup>1</sup>H} (125.8 MHz, CDCl<sub>3</sub>): δ 146.4 (=CH), 143.9 (OTs), 139.0 (OTs), 134.8 (=CH), 128.7 (C<sub>quart</sub>), 128.5 (OTs), 125.8 (OTs), 116.7 (=CH), 69.4 (CH<sub>2</sub>), 53.7 (N(CH<sub>3</sub>)<sub>2</sub>), 34.6 (CH<sub>2</sub>), 25.4 (OTs), 21.6, 21.2, 18.9, 13.6 (CH<sub>3</sub> and CH<sub>2</sub>). IR (neat): ν = 3030, 2959, 2928, 2871, 1665, 1455, 1378, 1192, 1118, 1033, 1011 cm<sup>-1</sup>. LRFAB-MS (+): *m/z* 182 [N<sup>+</sup>]. Anal. Calcd for C<sub>19</sub>H<sub>31</sub>NO<sub>3</sub>S: C, 64.55; H, 8.84; N, 3.96. Found: C, 64.18; H, 9.02; N, 4.16.

**[NMe<sub>2</sub>(*cis*-2-hexenyl)(CH=C(CH<sub>3</sub>)<sub>2</sub>)]<sup>+</sup>OTs<sup>-</sup> (6-OTs).** The product was isolated as a hygroscopic white powder in 94% yield (1.20 g, 3.53 mmol). <sup>1</sup>H NMR (500 MHz, CDCl<sub>3</sub>): δ 7.76 (d, <sup>3</sup>J = 8.1 Hz, 2H, OTs), 7.12 (d, <sup>3</sup>J = 7.9 Hz, 2H, OTs), 5.97 (dt, <sup>3</sup>J = 11.0 Hz, <sup>3</sup>J = 7.6 Hz, 1H, =CH), 5.84 (s, br, 1H, =CH), 5.46 (m, 1H, =CH), 4.35 (d, <sup>3</sup>J = 7.7 Hz, 2H, CH<sub>2</sub>), 3.49 (s, 6H, N(CH<sub>3</sub>)<sub>2</sub>), 2.32 (s, 3H, OTs), 2.13 (dq, <sup>3</sup>J = 7.3 Hz, <sup>4</sup>J = 1.2 Hz, 2H, CH<sub>2</sub>), 1.95 (d, <sup>4</sup>J = 1.3 Hz, 3H, CH<sub>3</sub>), 1.78 (d, <sup>4</sup>J = 1.3 Hz, 3H, CH<sub>3</sub>), 1.36 (sext., <sup>3</sup>J = 7.3 Hz, 2H, CH<sub>2</sub>), 0.86 (t, <sup>3</sup>J = 7.3 Hz, 3H, CH<sub>3</sub>). <sup>13</sup>C{<sup>1</sup>H} (125.8 MHz, CDCl<sub>3</sub>): δ 143.9 (OTs), 143.5 (=CH), 139.0 (OTs), 135.1 (=CH), 128.8 (C<sub>quart</sub>),

128.5 (OTs), 125.8 (OTs), 116.0 (=CH), 64.2 (CH<sub>2</sub>), 54.1 (N(CH<sub>3</sub>)<sub>2</sub>), 29.7 (CH<sub>2</sub>), 25.5 (OTs), 22.2, 21.2, 18.9, 13.6 (CH<sub>3</sub> and CH<sub>2</sub>). IR (neat): ν = 3023, 2967, 1657, 1493, 1458, 1210, 1191, 1118, 1033, 1010 cm<sup>-1</sup>. LRFAB-MS (+): *m/z* 182 [N<sup>+</sup>]. Anal. Calcd for C<sub>19</sub>H<sub>31</sub>NO<sub>3</sub>S: C, 64.55; H, 8.84; N, 3.96. Found: C, 64.29; H, 8.97; N, 4.20.

**[NMe<sub>2</sub>(4-methyl-2-*trans*-pentenyl)(CH=C(CH<sub>3</sub>)<sub>2</sub>)]<sup>+</sup>OTs<sup>-</sup> (7-OTs).** The product was isolated as a hygroscopic white solid in 92% yield (1.17 g, 3.46 mmol). <sup>1</sup>H NMR (500 MHz, CDCl<sub>3</sub>): δ 7.77 (d, <sup>3</sup>J = 8.1 Hz, 2H, OTs), 7.13 (d, <sup>3</sup>J = 7.9 Hz, 2H, OTs), 6.08 (dd, <sup>3</sup>J = 15.3 Hz, <sup>3</sup>J = 6.8 Hz, 1H, =CH), 5.81 (s, br, 1H, =CH), 5.38 (dtd, <sup>3</sup>J = 15.4 Hz, <sup>3</sup>J = 7.6 Hz, <sup>4</sup>J = 1.2 Hz, 1H, =CH), 4.30 (d, <sup>3</sup>J = 7.4 Hz, 2H, CH<sub>2</sub>), 3.46 (s, 6H, N(CH<sub>3</sub>)<sub>2</sub>), 2.35 (m, 1H, i-Pr), 2.33 (s, 3H, OTs), 1.95 (d, <sup>4</sup>J = 1.3 Hz, 3H, CH<sub>3</sub>), 1.79 (d, <sup>4</sup>J = 1.4 Hz, 3H, CH<sub>3</sub>), 0.98 (d, <sup>3</sup>J = 6.8 Hz, 3H, CH<sub>3</sub>). <sup>13</sup>C{<sup>1</sup>H} (125.8 MHz, CDCl<sub>3</sub>): δ 153.2 (=CH), 143.9 (OTs), 139.0 (OTs), 135.1 (=CH), 128.6 (C<sub>quart</sub>), 128.5 (OTs), 125.9 (OTs), 113.7 (=CH), 69.7 (CH<sub>2</sub>), 53.9 (N(CH<sub>3</sub>)<sub>2</sub>), 31.4, 25.5 (OTs), 25.5, 21.6, 21.3, 19.0 (CH<sub>3</sub> and CH). IR (neat): ν = 3027, 2965, 2869, 1494, 1461, 1191, 1120, 1032, 1010 cm<sup>-1</sup>. LRFAB-MS (+): *m/z* 182 [N<sup>+</sup>]. Anal. Calcd for C<sub>19</sub>H<sub>31</sub>NO<sub>3</sub>S: C, 64.55; H, 8.84; N, 3.96. Found: C, 64.36; H, 8.99; N, 4.08.

**[NMe<sub>2</sub>(*trans*-2-heptenyl)(CH=C(CH<sub>3</sub>)<sub>2</sub>)]<sup>+</sup>OTs<sup>-</sup> (8-OTs).** The product was isolated as a white solid in 90% yield (1.24 g, 3.38 mmol). <sup>1</sup>H NMR (500 MHz, CDCl<sub>3</sub>): δ 7.74 (d, <sup>3</sup>J = 8.0 Hz, 2H, OTs), 7.11 (d, <sup>3</sup>J = 7.9 Hz, 2H, OTs), 6.07 (dt, <sup>3</sup>J = 15.3 Hz, <sup>3</sup>J = 6.8 Hz, 1H, =CH), 5.80 (s, br, 1H, =CH), 5.39 (dt, <sup>3</sup>J = 15.3 Hz, <sup>3</sup>J = 7.4 Hz, 1H, =CH), 4.24 (d, <sup>3</sup>J = 7.4 Hz, 2H, CH<sub>2</sub>), 3.40 (s, 6H, N(CH<sub>3</sub>)<sub>2</sub>), 2.31 (s, 3H, OTs), 2.05 (q, <sup>3</sup>J = 7.0 Hz, 2H, CH<sub>2</sub>), 1.90 (d, <sup>4</sup>J = 1.2 Hz, 3H, CH<sub>3</sub>), 1.75 (d, <sup>4</sup>J = 1.2 Hz, 3H, CH<sub>3</sub>), 1.35–1.20 (m, 4H, CH<sub>2</sub>), 0.86 (t, <sup>3</sup>J = 7.1 Hz, 3H, CH<sub>3</sub>). <sup>13</sup>C{<sup>1</sup>H} (125.8 MHz, CDCl<sub>3</sub>): δ 146.7 (=CH), 143.9 (OTs), 139.0 (OTs), 134.9 (=CH), 128.7 (C<sub>quart</sub>), 128.5 (OTs), 125.8 (OTs), 116.5 (=CH), 65.8 (CH<sub>2</sub>), 53.7 (N(CH<sub>3</sub>)<sub>2</sub>), 32.3 (CH<sub>2</sub>), 30.5 (CH<sub>2</sub>), 25.5 (OTs), 22.2, 21.2, 18.9, 13.8 (CH<sub>3</sub> and CH<sub>2</sub>). LRFAB-MS (+): *m/z* 196 [N<sup>+</sup>]. Anal. Calcd for C<sub>20</sub>H<sub>33</sub>NO<sub>3</sub>S: C, 65.36; H, 9.05; N, 3.81. Found: C, 65.03; H, 9.20; N, 3.59.

**[NMe<sub>2</sub>(*trans*-3-(trimethylsilyl)allyl)(CH=C(CH<sub>3</sub>)<sub>2</sub>)]<sup>+</sup>OTs<sup>-</sup> (9-OTs).** The product was isolated as a white powder in 95% yield (1.37 g, 3.57 mmol). <sup>1</sup>H NMR (500 MHz, CDCl<sub>3</sub>): δ 7.79 (d, <sup>3</sup>J = 8.4 Hz, 2H, OTs), 7.14 (d, <sup>3</sup>J = 8.0 Hz, 2H, OTs), 6.42 (d, <sup>3</sup>J = 18.0 Hz, 1H, =CH), 5.93 (dt, <sup>3</sup>J = 18.2 Hz, <sup>3</sup>J = 7.0 Hz, 1H, =CH), 5.86 (s, br, 1H, =CH), 4.40 (d, <sup>3</sup>J = 6.5 Hz, 2H, CH<sub>2</sub>), 3.53 (s, 6H, N(CH<sub>3</sub>)<sub>2</sub>), 2.33 (s, 3H, OTs), 1.97 (d, <sup>4</sup>J = 1.2 Hz, 3H, CH<sub>3</sub>), 1.82 (d, <sup>4</sup>J = 1.2 Hz, 3H, CH<sub>3</sub>), 0.02 (s, 9H, TMS). <sup>13</sup>C{<sup>1</sup>H} (125.8 MHz, CDCl<sub>3</sub>): δ 147.7 (=CH), 143.8 (OTs), 139.1 (OTs), 135.0 (=CH), 131.1 (=CH), 128.7 (C<sub>quart</sub>), 128.5 (OTs), 125.9 (OTs), 71.5 (CH<sub>2</sub>), 54.2 (N(CH<sub>3</sub>)<sub>2</sub>), 25.5 (OTs), 21.3, 19.0 (CH<sub>3</sub>), -1.8 (TMS). LRFAB-MS (+): *m/z* 212 [N<sup>+</sup>]. Anal. Calcd for C<sub>19</sub>H<sub>33</sub>NO<sub>3</sub>SSi: C, 59.49; H, 8.67; N, 3.65. Found: C, 59.43; H, 8.77; N, 3.66.

**[NMe<sub>2</sub>(3,3-dimethylallyl)(CH=C(CH<sub>3</sub>)<sub>2</sub>)]<sup>+</sup>Br<sup>-</sup> (10-Br).** The product was isolated in 82% yield (765 mg, 3.08 mmol) as an off-white sticky residue which solidified upon cooling to -30 °C. <sup>1</sup>H NMR (500 MHz, CDCl<sub>3</sub>): δ 5.87 (s, br, 1H, =CH), 5.26 (t, <sup>3</sup>J = 7.9 Hz, 1H, =CH), 4.50 (d, <sup>3</sup>J = 7.9 Hz, 2H, CH<sub>2</sub>), 3.59 (s, 6H, N(CH<sub>3</sub>)<sub>2</sub>), 2.00 (d, <sup>4</sup>J = 1.3 Hz, 3H, CH<sub>3</sub>), 1.90 (s, 3H, CH<sub>3</sub>), 1.83 (s, 6H, 2 × CH<sub>3</sub>). <sup>13</sup>C{<sup>1</sup>H} (125.8 MHz, CDCl<sub>3</sub>): δ 148.6 (=CH), 135.2 (=CH), 128.8 (C<sub>quart</sub>), 111.3 (=CH), 65.6 (CH<sub>2</sub>), 53.8 (N(CH<sub>3</sub>)<sub>2</sub>), 26.4, 25.7, 19.5, 19.2 (4 × CH<sub>3</sub>). LRFAB-MS (+): *m/z* 168 [N<sup>+</sup>]. Anal. Calcd for C<sub>11</sub>H<sub>22</sub>BrN<sup>1/3</sup>H<sub>2</sub>O: C, 51.91; H, 8.99; N, 5.51. Found: C, 51.82; H, 8.98; N, 5.55.

**General Procedure for Encapsulation Reactions.** K<sub>6</sub>(NMe<sub>4</sub>)<sub>5</sub>-[NMe<sub>4</sub>CGa<sub>4</sub>L<sub>6</sub>] (26.3 mg, 7.50 μmol) and the enammonium salt (7.50 μmol) were combined in a vial and dissolved in 500 μL of cold D<sub>2</sub>O. The solution was transferred to an NMR tube and the spectrum recorded within 5 min after dissolution. Due to the reactive nature of these host-guest complexes, the complexes were only characterized in solution. Representative mass spectrometry data for the allyl enammonium host-guest complexes is given for host-guest complex Na<sub>11</sub>[1CGa<sub>4</sub>L<sub>6</sub>]. The

utilization of Na<sup>+</sup> as the counterion has the advantage of providing a less complicated isotope pattern, thus leading to better signal intensities.

**Data for Host–Guest Complexes, Prepared As Described Above.**

**K<sub>5</sub>(NMe<sub>4</sub>)<sub>6</sub>[1C-Ga<sub>4</sub>L<sub>6</sub>].** <sup>1</sup>H NMR (500 MHz, D<sub>2</sub>O): δ 13.50 (s, 12H, N–H), 7.95 (s, br, 12H, Ar–H), 7.77 (s, br, 12H, Ar–H), 7.25 (d, <sup>3</sup>J = 7.9 Hz, 12H, Ar–H), 7.02 (t, <sup>3</sup>J = 8.0 Hz, 12H, Ar–H), 6.70 (d, <sup>3</sup>J = 7.2 Hz, 12H, Ar–H), 6.56 (t, <sup>3</sup>J = 7.7 Hz, 12H, Ar–H), 3.09 (d, <sup>3</sup>J = 7.2 Hz, 1H, =CH<sub>2</sub>, encaps.), 2.65 (s, 72H, NMe<sub>4</sub>, exterior), 2.44 (s, br, 1H, =CH, encaps.), 2.32 (m, 1H, =CH, encaps.), 0.24 (s, 3H, CH<sub>3</sub>, encaps.), 0.21 (m, 1H, CH<sub>2</sub>, encaps.), 0.05 (m, 1H, CH<sub>2</sub>, encaps.), –0.03 (s, 3H, CH<sub>3</sub>, encaps.), –0.60 (s, 3H, CH<sub>3</sub>, encaps.), –1.08 (s, 3H, CH<sub>3</sub>, encaps.). ES(–)-MS (H<sub>2</sub>O/MeOH, 50:50) (♦ = [Ga<sub>4</sub>L<sub>6</sub>]<sup>12–</sup>): *m/z* 605 [N<sup>+</sup>C♦ + 2Na<sup>+</sup> + 4H<sup>+</sup>]<sup>5–</sup>, 610 [N<sup>+</sup>C♦ + 3Na<sup>+</sup> + 3H<sup>+</sup>]<sup>5–</sup>, 614 [N<sup>+</sup>C♦ + 4Na<sup>+</sup> + 2H<sup>+</sup>]<sup>5–</sup>, 619 [N<sup>+</sup>C♦ + 5Na<sup>+</sup> + 1H<sup>+</sup>]<sup>5–</sup>, 623 [N<sup>+</sup>C♦ + 6Na<sup>+</sup>]<sup>5–</sup>, 764 [N<sup>+</sup>C♦ + 3Na<sup>+</sup> + 4H<sup>+</sup>]<sup>4–</sup>, 769 [N<sup>+</sup>C♦ + 4Na<sup>+</sup> + 3H<sup>+</sup>]<sup>4–</sup>, 774 [N<sup>+</sup>C♦ + 5Na<sup>+</sup> + 2H<sup>+</sup>]<sup>4–</sup>, 780 [N<sup>+</sup>C♦ + 6Na<sup>+</sup> + 1H<sup>+</sup>]<sup>4–</sup>, 785 [N<sup>+</sup>C♦ + 7Na<sup>+</sup>]<sup>4–</sup>, 1017 [N<sup>+</sup>C♦ + 3Na<sup>+</sup> + 5H<sup>+</sup>]<sup>3–</sup>, 1024 [N<sup>+</sup>C♦ + 4Na<sup>+</sup> + 4H<sup>+</sup>]<sup>3–</sup>, 1032 [N<sup>+</sup>C♦ + 5Na<sup>+</sup> + 3H<sup>+</sup>]<sup>3–</sup>, 1039 [N<sup>+</sup>C♦ + 6Na<sup>+</sup> + 2H<sup>+</sup>]<sup>3–</sup>, 1046 [N<sup>+</sup>C♦ + 7Na<sup>+</sup> + 1H<sup>+</sup>]<sup>3–</sup>, 1054 [N<sup>+</sup>C♦ + 8Na<sup>+</sup>]<sup>3–</sup>.

**K<sub>5</sub>(NMe<sub>4</sub>)<sub>6</sub>[2C-Ga<sub>4</sub>L<sub>6</sub>].** <sup>1</sup>H NMR (500 MHz, D<sub>2</sub>O): δ 13.44 (s, 12H, N–H), 7.90 (s, br, 12H, Ar–H), 7.68 (s, br, 12H, Ar–H), 7.18 (d, <sup>3</sup>J = 8.0 Hz, 12H, Ar–H), 6.93 (t, <sup>3</sup>J = 7.8 Hz, 12H, Ar–H), 6.62 (d, <sup>3</sup>J = 7.0 Hz, 12H, Ar–H), 6.48 (t, <sup>3</sup>J = 7.5 Hz, 12H, Ar–H), 2.52 (s, 72H, NMe<sub>4</sub>, exterior), 2.38 (s, br, 1H, =CH, encaps.), 1.63 (s, br, 1H, =CH, encaps.), 0.89 (s, br, 1H, =CH, encaps.), 0.34 (s, 3H, CH<sub>3</sub>, encaps.), 0.21 (d, <sup>3</sup>J = 12.5 Hz, 1H, CH<sub>2</sub>, encaps.), 0.08 (d, <sup>3</sup>J = 12.5 Hz, 1H, CH<sub>2</sub>, encaps.), –0.24 (s, 3H, CH<sub>3</sub>, encaps.), –0.48 (s, 3H, CH<sub>3</sub>, encaps.), –1.24 (s, 6H, 2 × CH<sub>3</sub>, encaps.).

**K<sub>5</sub>(NMe<sub>4</sub>)<sub>6</sub>[3C-Ga<sub>4</sub>L<sub>6</sub>].** <sup>1</sup>H NMR (500 MHz, D<sub>2</sub>O): δ 13.48 (s, 12H, N–H), 7.91 (s, br, 12H, Ar–H), 7.63 (s, br, 12H, Ar–H), 7.17 (d, <sup>3</sup>J = 8.0 Hz, 12H, Ar–H), 6.89 (t, <sup>3</sup>J = 7.9 Hz, 12H, Ar–H), 6.61 (d, <sup>3</sup>J = 7.5 Hz, 12H, Ar–H), 6.46 (t, <sup>3</sup>J = 7.5 Hz, 12H, Ar–H), 2.55 (s, 72H, NMe<sub>4</sub>, exterior), 2.31 (m, br, 1H, =CH, encaps.), 1.54 (s, br, 1H, =CH, encaps.), 1.34 (m, br, 1H, =CH, encaps.), 0.68 (s, 3H, CH<sub>3</sub>, encaps.), 0.38 (m, br, 1H, CH<sub>2</sub>, encaps.), 0.31 (s, 3H, CH<sub>3</sub>, encaps.), 0.22 (s, 3H, CH<sub>3</sub>, encaps.), –0.07 (m, br, 1H, CH<sub>2</sub>, encaps.), –0.42 (m, br, 1H, CH<sub>2</sub>, encaps.), –0.57 (m, br, 1H, CH<sub>2</sub>, encaps.), –1.07 (t, br, 3H, CH<sub>3</sub>), –1.28 (s, 3H, CH<sub>3</sub>, encaps.).

**K<sub>5</sub>(NMe<sub>4</sub>)<sub>6</sub>[4C-Ga<sub>4</sub>L<sub>6</sub>].** <sup>1</sup>H NMR (500 MHz, D<sub>2</sub>O): δ 13.45 (s, 12H, N–H), 7.93 (s, br, 12H, Ar–H), 7.65 (s, br, 12H, Ar–H), 7.18 (d, <sup>3</sup>J = 8.0 Hz, 12H, Ar–H), 6.89 (t, <sup>3</sup>J = 7.7 Hz, 12H, Ar–H), 6.61 (d, <sup>3</sup>J = 7.4 Hz, 12H, Ar–H), 6.47 (t, <sup>3</sup>J = 7.5 Hz, 12H, Ar–H), 2.82 (m, br, 1H, =CH, encaps.), 2.56 (s, 72H, NMe<sub>4</sub>, exterior), 2.29 (s, br, 1H, =CH, encaps.), 2.19 (m, br, 1H, =CH, encaps.), 0.73 (s, 3H, CH<sub>3</sub>, encaps.), 0.36 (m, br, 1H, CH<sub>2</sub>, encaps.), 0.14 (m, 2H, CH<sub>2</sub>), –0.42 (s, 3H, CH<sub>3</sub>, encaps.), –1.03 (s, 3H, CH<sub>3</sub>, encaps.), –1.13 (t, br, 3H, CH<sub>3</sub>), –1.32 (m, 2H, CH<sub>2</sub>, encaps.).

**K<sub>5</sub>(NMe<sub>4</sub>)<sub>6</sub>[5C-Ga<sub>4</sub>L<sub>6</sub>].** <sup>1</sup>H NMR (500 MHz, D<sub>2</sub>O): δ 13.42 (s, 12H, N–H), 7.88 (s, br, 12H, Ar–H), 7.65 (s, br, 12H, Ar–H), 7.15 (d, <sup>3</sup>J = 8.0 Hz, 12H, Ar–H), 6.87 (s, br, 12H, Ar–H), 6.61 (d, <sup>3</sup>J = 7.7 Hz, 12H, Ar–H), 6.46 (t, <sup>3</sup>J = 7.5 Hz, 12H, Ar–H), 3.11 (s, br, 1H, =CH, encaps.), 2.54 (s, 72H, NMe<sub>4</sub>, exterior), 1.76 (s, br, 1H, =CH, encaps.), 0.90 (s, 3H, CH<sub>3</sub>, encaps.), 0.38 (s, 3H, CH<sub>3</sub>, encaps.), 0.31 (m, br, 1H, CH<sub>2</sub>, encaps.), 0.16 (m, br, 1H, CH<sub>2</sub>, encaps.), –0.21 (s, br, 3H, CH<sub>3</sub>, encaps.), –0.46 (m, br, 1H, CH<sub>2</sub>, encaps.), –0.89 (s, br, 4H, CH<sub>3</sub> and CH<sub>2</sub>, encaps.), –1.14 (s, br, 3H, CH<sub>3</sub>, encaps.), –1.58 (m, br, 2H, CH<sub>2</sub>, encaps.).

**K<sub>5</sub>(NMe<sub>4</sub>)<sub>6</sub>[6C-Ga<sub>4</sub>L<sub>6</sub>].** <sup>1</sup>H NMR (500 MHz, D<sub>2</sub>O): δ 13.45 (s, 12H, N–H), 8.03 (s, br, 12H, Ar–H), 7.73 (s, br, 12H, Ar–H), 7.26 (s, br, 12H, Ar–H), 6.96 (s, br, 12H, Ar–H), 6.70 (s, br, 12H, Ar–H), 6.57 (s, br, 12H, Ar–H), 3.58 (m, br, 1H, =CH, encaps.), 2.52 (s, 72H, NMe<sub>4</sub>, exterior), 2.42 (m, br, 1H, =CH, encaps.), 1.37 (s, br, 1H, =CH, encaps.), 0.79 (s, br, 3H, CH<sub>3</sub>, encaps.), 0.61 (s, br, 3H, CH<sub>3</sub>, encaps.), 0.42 (m, br, 1H, CH<sub>2</sub>, encaps.), 0.14 (m, br, 1H, CH<sub>2</sub>, encaps.), –0.33 (s, br, 3H, CH<sub>3</sub>, encaps.), –0.95 (s, br, 3H, CH<sub>3</sub>, encaps.), –1.11

(s, br, 3H, CH<sub>3</sub>, encaps.), –1.37 (m, br, 1H, CH<sub>2</sub>, encaps.), –1.42 (m, br, 1H, CH<sub>2</sub>, encaps.), –1.53 (m, br, 1H, CH<sub>2</sub>, encaps.), –1.64 (m, br, 1H, CH<sub>2</sub>, encaps.).

**K<sub>5</sub>(NMe<sub>4</sub>)<sub>6</sub>[7C-Ga<sub>4</sub>L<sub>6</sub>].** <sup>1</sup>H NMR (500 MHz, D<sub>2</sub>O): δ 13.47 (s, 12H, N–H), 8.05 (s, br, 12H, Ar–H), 7.69 (s, br, 12H, Ar–H), 7.26 (s, br, 12H, Ar–H), 6.97 (s, br, 12H, Ar–H), 6.70 (s, br, 12H, Ar–H), 6.56 (s, br, 12H, Ar–H), 2.70 (m, br, 1H, =CH, encaps.), 2.52 (s, 72H, NMe<sub>4</sub>, exterior), 1.84 (s, br, 1H, =CH, encaps.), 1.66 (m, br, 1H, =CH, encaps.), 0.93 (s, br, 3H, CH<sub>3</sub>, encaps.), 0.85 (s, br, 3H, CH<sub>3</sub>, encaps.), 0.69 (m, br, 1H, CH<sub>2</sub>, encaps.), 0.49 (s, br, 3H, CH<sub>3</sub>, encaps.), –0.42 (m, br, 1H, CH<sub>2</sub>, encaps.), –1.32 (s, br, 3H, CH<sub>3</sub>, encaps.), –1.63 (s, br, 3H, CH<sub>3</sub>, encaps.), –1.71 (s, br, 3H, CH<sub>3</sub>, encaps.), –1.79 (m, br, 1H, CH, encaps.).

**K<sub>5</sub>(NMe<sub>4</sub>)<sub>6</sub>[8C-Ga<sub>4</sub>L<sub>6</sub>].** <sup>1</sup>H NMR (500 MHz, D<sub>2</sub>O): δ 13.41 (s, 12H, N–H), 7.94 (s, br, 12H, Ar–H), 7.77 (s, br, 12H, Ar–H), 7.24 (s, br, 12H, Ar–H), 6.99 (s, br, 12H, Ar–H), 6.70 (s, br, 12H, Ar–H), 6.56 (s, br, 12H, Ar–H), 2.50 (s, br, 72H, NMe<sub>4</sub>, exterior), 1.6 – (–1.4) (many broad multiplets, not resolved, encapsulated substrate).

**K<sub>5</sub>(NMe<sub>4</sub>)<sub>6</sub>[9C-Ga<sub>4</sub>L<sub>6</sub>].** <sup>1</sup>H NMR (500 MHz, D<sub>2</sub>O): δ 13.46 (s, 12H, N–H), 7.93 (d, <sup>3</sup>J = 7.6 Hz, 12H, Ar–H), 7.88 (d, <sup>3</sup>J = 8.5 Hz, 12H, Ar–H), 7.28 (d, <sup>3</sup>J = 7.4 Hz, 12H, Ar–H), 7.13 (t, <sup>3</sup>J = 8.1 Hz, 12H, Ar–H), 6.75 (dd, <sup>3</sup>J = 7.3 Hz, <sup>4</sup>J = 1.3 Hz 12H, Ar–H), 6.60 (t, <sup>3</sup>J = 7.8 Hz, 12H, Ar–H), 2.52 (s, br, 72H, NMe<sub>4</sub>, exterior), 3.3 – (–1.2) (many broad resonances, not resolved, encapsulated substrate).

**K<sub>5</sub>(NMe<sub>4</sub>)<sub>6</sub>[10C-Ga<sub>4</sub>L<sub>6</sub>].** <sup>1</sup>H NMR (500 MHz, D<sub>2</sub>O): δ 13.59 (s, 12H, N–H), 8.08 (s, br, 12H, Ar–H), 7.83 (s, br, 12H, Ar–H), 7.34 (d, <sup>3</sup>J = 8.0 Hz, 12H, Ar–H), 7.08 (t, <sup>3</sup>J = 7.9 Hz, 12H, Ar–H), 6.77 (d, <sup>3</sup>J = 7.2 Hz, 12H, Ar–H), 6.62 (t, <sup>3</sup>J = 7.6 Hz, 12H, Ar–H), 2.54 (s, 72H, NMe<sub>4</sub>, exterior), 1.72 (m, br, 1H, =CH, encaps.), 1.29 (s, 1H, =CH, encaps.), 0.41 (s, 3H, CH<sub>3</sub>, encaps.), 0.35 (m, 2H, CH<sub>2</sub>, encaps.), 0.29 (s, 6H, 2 × CH<sub>3</sub>, encaps.), 0.16 (s, 3H, CH<sub>3</sub>, encaps.), –1.42 (s, 3H, CH<sub>3</sub>, encaps.), –1.51 (s, 3H, CH<sub>3</sub>, encaps.).

**K<sub>5</sub>(NMe<sub>4</sub>)<sub>6</sub>[10iC-Ga<sub>4</sub>L<sub>6</sub>].** <sup>1</sup>H NMR (500 MHz, D<sub>2</sub>O, N–H not observed due to H–D exchange): δ 8.12 (d, <sup>3</sup>J = 7.5 Hz, 12H, Ar–H), 7.83 (d, <sup>3</sup>J = 8.4 Hz, 12H, Ar–H), 7.29 (d, <sup>3</sup>J = 8.3 Hz, 12H, Ar–H), 7.04 (t, <sup>3</sup>J = 8.0 Hz, 12H, Ar–H), 6.76 (d, <sup>3</sup>J = 7.5 Hz, 12H, Ar–H), 6.62 (t, <sup>3</sup>J = 7.6 Hz, 12H, Ar–H), 4.35 (s, 1H, =CH, encaps.), 3.91 (d, <sup>3</sup>J = 10.5 Hz, 1H, =CH, encaps.), 2.56 (s, 72H, NMe<sub>4</sub>, exterior), 2.30 (m, 1H, =CH, encaps.), 1.67 (s, 3H, NMe<sub>2</sub>, encaps.), 0.86 (s, 3H, NMe<sub>2</sub>, encaps.), –1.86 (s, 3H, CH<sub>3</sub>, encaps.), –2.02 (s, 3H, CH<sub>3</sub>, encaps.), –2.20 (s, 3H, CH<sub>3</sub>, encaps.), –2.24 (s, 3H, CH<sub>3</sub>, encaps.).

**Kinetic Runs of Enammonium Substrates.** Kinetic runs were performed in D<sub>2</sub>O on a Bruker AVB 400 or DRX 500 MHz spectrometer. The concentration of all samples was 15 mM, and the solutions were buffered with 150 mM phosphate buffer, adjusted to pD 8.00. Sealed capillaries containing a D<sub>2</sub>O/dioxane mixture served as internal standard for integration. Temperatures in the probe were measured with an ethylene glycol standard.

**NOE Growth Rates.** Samples of [3C-Ga<sub>4</sub>L<sub>6</sub>]<sup>11–</sup> and [4C-Ga<sub>4</sub>L<sub>6</sub>]<sup>11–</sup> were prepared as 15 mM solutions in a D<sub>2</sub>O/MeOD mixture (70:30). 2D NOESY spectra were recorded at –10 °C on a Bruker Avance AV 500 spectrometer, with varying mixing times (20, 40, 65, 90, 120, 150, 200, 300, 500, 750, and 1000 ms). NOE cross-peak intensity was plotted versus mixing time (τ<sub>m</sub>). Using the geminal diastereotopic methylene protons as a known internal reference distance *r*<sub>XY</sub> (1.75 Å), the NOE growth rates σ for the unknown distances could be quantitated, according to *r*<sub>AB</sub> = *r*<sub>XY</sub>(σ<sub>XY</sub>/σ<sub>AB</sub>)<sup>1/6</sup>.<sup>46</sup> Methyl groups are treated as rapid rotors, and NOE growth rates for methyl groups are divided by 3 to account for the presence of three correlating protons. Distances to methyl groups are reported relative to a pseudoatom located in the center of the plane of the three protons.

**Variable pD Kinetics.** All solutions were prepared in D<sub>2</sub>O containing 10 mM K<sub>5</sub>(NMe<sub>4</sub>)<sub>6</sub>[10C-Ga<sub>4</sub>L<sub>6</sub>] and 100 mM of the different buffer solutions. Solutions were buffered at pD 6.5, 7.7, 8.1, 8.3 (phosphate buffer), 8.5, 8.6, 8.8, 9.1 (tris buffer), 9.7, 10.1, 10.3, 10.5, 10.6, 11.1

(carbonate buffer), and 12.8 (KOD). The standard conversion for the pH-calibrated electrode of  $pD = pH + 0.4$  was employed.<sup>61</sup> The pD was adjusted using either KOD (1 M in D<sub>2</sub>O) or DCl (1 M in D<sub>2</sub>O). The pD was remeasured after each kinetic run and remained constant for all samples. The pD was not corrected for temperature. Kinetic runs were performed on a Bruker DRX 500 MHz spectrometer at 50 °C ( $\pm 0.2$  °C). Sealed capillaries containing a D<sub>2</sub>O/dioxane mixture served as internal standard for integration. Temperatures in the probe were measured before each kinetic run with an ethylene glycol standard.

**Variable NMe<sub>4</sub><sup>+</sup> Kinetics.** All solutions were prepared using 0.01 M KOD in D<sub>2</sub>O, and the overall ionic strength was kept at 0.5 M with added KCl. For each sample, 300  $\mu$ L of a stock solution of K<sub>11</sub>[10C-Ga<sub>4</sub>L<sub>6</sub>] (16.67 mM) was combined with 0–100  $\mu$ L of an NMe<sub>4</sub>-Br solution (1.00 M) and 66–100  $\mu$ L of a 2.5 M KCl solution, so that the overall ionic strength of NMe<sub>4</sub><sup>+</sup> and K<sup>+</sup> amounted to 0.5 M. All samples were brought to a total volume of 500  $\mu$ L and transferred to an NMR tube. Kinetic runs were performed on a Bruker DRX 500 MHz spectrometer at 50 °C ( $\pm 0.2$  °C). Sealed capillaries containing a D<sub>2</sub>O/dioxane mixture served as internal standard for integration. Temperatures in the probe were measured before each kinetic run with an ethylene glycol standard.

**Variable NBu<sub>4</sub><sup>+</sup> Kinetics.** All solutions were prepared using 0.5 M KCl in D<sub>2</sub>O, containing 0.01 M KOD. For each sample, 400  $\mu$ L of

a stock solution of K<sub>11</sub>[10C-Ga<sub>4</sub>L<sub>6</sub>] (12.5 mM) was combined with 0–55  $\mu$ L of a 0.10 M NBu<sub>4</sub>Cl solution (precipitation occurred at higher temperatures when more than 55  $\mu$ L of NBu<sub>4</sub>Cl was added). All samples were adjusted to a total volume of 500  $\mu$ L and transferred to an NMR tube. Kinetic runs were performed on a Bruker DRX 500 MHz spectrometer at 50 °C ( $\pm 0.2$  °C). Sealed capillaries containing a D<sub>2</sub>O/dioxane mixture served as internal standard for integration. Temperatures in the probe were measured before each kinetic run with an ethylene glycol standard.

**Acknowledgment.** The authors thank Dennis H. Leung, Dr. Gojko Lalic, and Dr. Anna V. Davis for helpful discussions. This work was supported by the Director, Office of Energy Research, Office of Basic Energy Sciences, Chemical Sciences Division, of the U.S. Department of Energy under contract DE-AC03-7600098.

**Supporting Information Available:** Eyring plots for **3** and [3C-Ga<sub>4</sub>L<sub>6</sub>]<sup>11-</sup>; 2D NOESY spectrum of [3C-Ga<sub>4</sub>L<sub>6</sub>]<sup>11-</sup>; dependence of hydrolysis on NBu<sub>4</sub><sup>+</sup> concentration; displacement of **10i** from the cavity interior with NEt<sub>4</sub><sup>+</sup>; independence of the initial rearrangement step on pD and NMe<sub>4</sub><sup>+</sup> concentration. This material is available free of charge via the Internet at <http://pubs.acs.org>.

JA062329B

(61) Perrin, D. D.; Dempsey, B. *Buffers for pH and Metal Ion Control*; Chapman and Hall: London, 1974.